Towards Embodiment Scaling Laws in Robot Locomotion

Bo Ai[1*] **Liu Dai**[1*] **Nico Bohlinger**[4*] **Dichen Li**[1*] **Tongzhou Mu**[1]
Zhanxin Wu[3] **K. Fay**[1] **Henrik I. Christensen**[1] **Jan Peters**[4,5] **Hao Su**[1,2]
[1]University of California San Diego, USA [2]Hillbot Inc, USA
[3]Cornell University, USA [4]Technical University of Darmstadt, Germany
[5]German Research Center for AI (DFKI); Robotics Institute Germany; hessian.AI, Germany
https://embodiment-scaling-laws.github.io

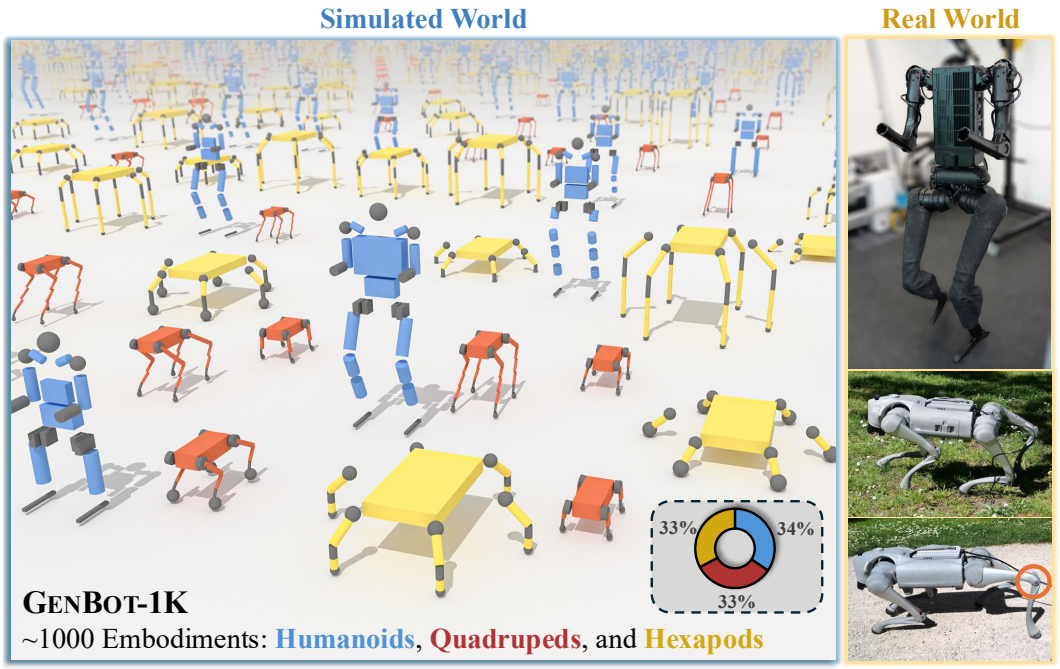

Figure 1: **One Policy, Two Worlds, Many Robots.** We study embodiment scaling laws by training a single policy on ∼1,000 procedurally generated "blueprint" embodiments in simulation. Our policy zero-shot transfers to real-world embodiments, including modified joint constraints (circled in red).

Abstract: Cross-embodiment generalization underpins the vision of building generalist embodied agents for *any* robot, yet its enabling factors remain poorly understood. We investigate *embodiment scaling laws*, the hypothesis that increasing the number of training embodiments improves generalization to unseen ones, using robot locomotion as a test bed. We procedurally generate ∼1,000 embodiments with topological, geometric, and joint-level kinematic variations, and train policies on random subsets. We observe positive scaling trends supporting the hypothesis, and find that embodiment scaling enables substantially broader generalization than data scaling on fixed embodiments. Our best policy, trained on the full dataset, transfers zero-shot to novel embodiments in simulation and the real world, including the Unitree Go2 and H1. These results represent a step toward general embodied intelligence, with relevance to adaptive control for configurable robots, morphology co-design, and beyond.

Keywords: Cross-Embodiment Learning, Robot Locomotion, Robotic Foundation Models, Reinforcement Learning, Behavior Cloning

* Equal contribution. Correspondence addressed to Bo Ai ⟨bai@ucsd.edu⟩.

9th Conference on Robot Learning (CoRL 2025), Seoul, Korea.

1 Introduction

Two millennia ago, Heraclitus wrote that no one steps into the same river twice. Today, one might say that no agent acts with exactly the same body twice. Robotic embodiments change with injury, aging, tool use, manufacturing variation, and upgrades, and this variability will only grow as robots become more capable and widely deployed in the real world. Leveraging heterogeneous deployment data and understanding how to apply learned policies to novel, unseen embodiments would be instrumental to building generalist robots via data flywheels. However, it is unclear how to enable policies to transfer across a large number of distinct embodiments.

Scaling has been a key driver of progress in deep learning, which can occur along multiple **dimensions**. Scaling **dataset size** and **model size** has improved generalization in vision [1–8] and language [9–18]. In robotics, scaling the number of **tasks** [19–28] and **environments** [22, 24, 25, 28–38] enable cross-task and cross-environment generalization. In this work, we explore a distinct and underexplored dimension of scaling: **robot embodiment**, the physical structure of robots. We hypothesize that scaling the number of training embodiments leads to better generalization to unseen embodiments, as the policies learn to capture shared control strategies across different physical structures. We conceptualize this hypothesized relationship as ***embodiment scaling laws***.

Studying this hypothesis requires addressing several open challenges. First, policy architectures need to (i) incorporate embodiment structure, (ii) adapt to varied observation and action spaces, and (iii) scale to large numbers of embodiments. Second, scaling experiments demand a large dataset of robot embodiments. We postulate that at least $\sim 10^3$ embodiments are needed to reveal a glimpse of long-term trends, whereas existing literature is limited to $\sim 10^1$ in the real world [21, 27–30, 38, 39] and $\sim 10^2$ in simulation [40]. Achieving this scale requires scalable and safe training and evaluation, which is only feasible in simulation at this point in time.

In simulation, we adopt a controlled setup to provide the first empirical validation of embodiment scaling laws. Proprioceptive locomotion serves as a foundational testbed: it has a small sim-to-real gap, depends primarily on morphology and dynamics, and avoids confounding factors from perception such as camera viewpoint, visual encoding, or rendering fidelity. We procedurally generate GenBot-1K, a collection of $\sim$1,000 blueprint robot descriptions, spanning humanoids, quadrupeds, and hexapods, by varying topology, geometry, and joint-level kinematic constraints. To handle varied state and action spaces, we extend Unified Robot Morphology Architecture (URMA) [41] into a wider multi-head attention architecture. We adopt a two-stage learning framework [42, 43] for scalable cross-embodiment learning: (i) train single-embodiment expert policies with Reinforcement Learning (RL), and (ii) distill these experts into a single embodiment-aware URMA policy via behavior cloning (BC). By varying the number of embodiments used for BC, we quantify the effect of embodiment scaling on generalization to unseen embodiments.

Overall, we present a large-scale empirical study of embodiment scaling laws across $\sim$1,000 robot embodiments. We design a general reward formulation, training curriculum, and domain randomization that enable scalable training of RL expert policies without embodiment-specific tuning, accumulating a total of 2 trillion simulation steps. We observe positive scaling trends supporting the hypothesis, and find that embodiment scaling enables substantially broader generalization than data scaling on fixed embodiments. The best policy, trained on 2 billion expert demonstration steps across the full set of training embodiments, zero-shot transfers to real-world robots, including the Unitree Go2 with varied kinematic constraints and the H1 humanoid. The findings underscore the potential of embodiment scaling for general embodied intelligence, and open up opportunities for embodiment-adaptive control, morphology co-design, and beyond.

2 Related Work

Cross-embodiment generalization. One goal of cross-embodiment learning is to enable control policies to generalize across robot embodiments without retraining. Prior efforts often focus on transferring policies between a small number of robots by aligning dynamics, learning shared em-

beddings [44, 45], or extracting transferable skills [46, 47]. However, these methods are only able to transfer to a single or a few target embodiments. Related work about scalable network architectures, such as graph neural networks [48, 49] or Transformers [50, 51], scale to more complex embodiments by conditioning on embodiment-specific information, but these works mostly use unrealistic and simplified robots that are not suitable for real-world transfer. More recent approaches can be trained on a larger number of realistic robot embodiments, but they often rely on existing low-level controllers [52, 53], embodiment-specific decoders [54], other action abstractions [55, 56], or assume a fixed observation and action space [57], limiting their generalization capabilities to predefined morphological structures. URMA [41] solves this issue by introducing a unified joint-level control architecture for arbitrary robot morphologies, but is validated only on 16 robots without studying scaling effects. Our work demonstrates broader cross-embodiment generalization than prior works by training a single policy on $\sim$1,000 embodiments, achieving zero-shot transfer to unseen embodiments in both simulation and the real world.

Robot locomotion. In recent years, Deep Reinforcement Learning (DRL) has been applied to single embodiment robot locomotion to great success. The combination of scalable on-policy RL algorithms, such as Proximal Policy Optimization (PPO) [58], with fast and highly parallelizable simulators has enabled the training of powerful locomotion policies for quadruped [59–65] and humanoid robots [66–70]. Techniques such as student-teacher learning [71, 72], curriculum learning [73–75], and domain randomization [73, 76, 77] have enabled zero-shot sim-to-real transfer of these policies. Less data-hungry methods for learning directly on real robots, utilizing model-based or off-policy RL algorithms [78–81], and non-learning methods, such as Model Predictive Control (MPC) [82, 83], have also been proposed for legged locomotion, but generally trade their efficiency for worse performance with less robust gaits on challenging terrain or under strong perturbations.

Robot embodiment generation. Prior research in robot embodiment generation has pursued several directions. One prominent direction focuses on optimizing robot designs for specific tasks, where procedural and learning-based techniques generate embodiments tailored for enhanced performance in tasks such as locomotion [84–86] or manipulation [87]. Closer to our objectives is the use of embodiment generation to develop generalizable robot policies. Existing works have explored methods based on simplified kinematic trees [51, 88], randomization within a fixed morphology [57], diverse sensor configurations [56], or varied hand structures [89]. However, these approaches are generally limited to a single robot class or topological template. In contrast, we introduce a comprehensive procedural generation framework that spans multiple morphology classes, including quadrupeds, hexapods, and humanoids, while varying topology, geometry, and kinematics for each of them. This enables a large-scale systematic study of embodiment scaling in locomotion.

3 Methodology

Generalizable cross-embodiment robot learning aims to train a control policy that can control diverse *seen* and *unseen* robot embodiments to solve a common task. Formally, let $\mathcal{E}$ denote a set of embodiments sampled from $\mathcal{P}_{\mathcal{E}}$, where each embodiment $e \in \mathcal{E}$ is defined as a triplet $e = \langle \mathcal{G}, \mathcal{T}, \mathcal{K} \rangle$, where $\mathcal{T}$ specifies the joint topology (i.e., number and connectivity), $\mathcal{G}$ denotes link geometry (e.g., shape and size), and $\mathcal{K}$ describes additional kinematic properties (e.g., joint types and range of motion). The control problem of each embodiment e is defined by a Markov Decision Process (MDP) $\mathcal{M}_e = \langle \mathcal{S}_e, \mathcal{A}_e, P_e, R_e, H \rangle$, where $\mathcal{S}_e$, $\mathcal{A}_e$, and P_e denote the state space, action space, and transition dynamics; R_e is the reward function; and H is the episode horizon. At any particular time step t, a policy predicts an action $a_t \in \mathcal{A}_e$, conditioned on the robot state $s_t \in \mathcal{S}_e$ and the embodiment descriptor $\phi(e)$. In the specific case of robot locomotion, the policy is additionally conditioned on a x-y-yaw velocity command $v_t \in \mathbb{R}^3$ with respect to the trunk frame, i.e., $a_t \sim \pi(s_t, \phi(e), v_t)$.

During training, we optimize the policy to maximize the expected cumulative reward across training embodiments $\mathcal{E}_{\text{train}} \subset \mathcal{E}$ with trajectories $\tau = \{(s_0, a_0), \ldots, (s_H, a_H)\}$ sampled from $\mathcal{M}_e$:

$$\pi^*_{\text{train}} = \arg\max_{\pi} \mathbb{E}_{e \in \mathcal{E}_{\text{train}}} \mathbb{E}_{\tau \sim \pi} \left[\sum_{t=0}^{H} R_e(s_t, v_t, a_t) \right]. \tag{1}$$

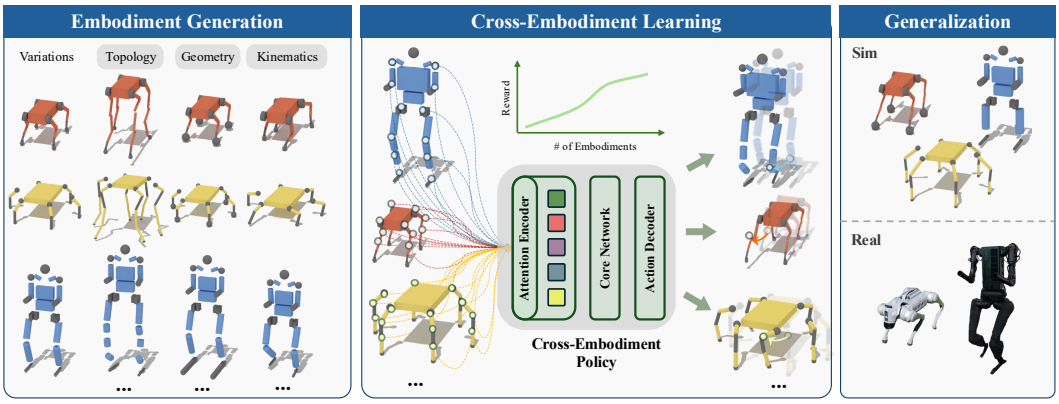

Figure 2: **Overview of our approach for studying embodiment scaling laws.** We procedurally generate GENBOT-1K, a dataset of ∼1000 diverse robot embodiments with structured variations in topology, geometry, and kinematics. We train a single cross-embodiment policy using the URMA architecture, which handles varying observation and action spaces via attention-based joint encoding. We systematically vary the number of training embodiments to study how generalization scales with embodiment quantity. The policy trained on the full training dataset transfers zero-shot to novel simulated robots and real-world hardware with different morphologies.

The generalization performance is evaluated on a held-out set of embodiments $\mathcal{E}_{\text{test}} = \mathcal{E} \setminus \mathcal{E}_{\text{train}}$:

$$J_{\text{test}}(\pi^*_{\text{train}}) = \mathbb{E}_{e \in \mathcal{E}_{\text{test}}} \mathbb{E}_{\tau \sim \pi^*_{\text{train}}} \left[\sum_{t=0}^{H} R_e(s_t, v_t, a_t) \right]. \tag{2}$$

We note that both *learning* and *generalizing* across embodiments present significant challenges. Differing observation and action spaces require policies to handle variable-sized and structurally different inputs and outputs. Variations in kinematic constraints, self-collision profiles, and contact dynamics introduce embodiment-specific behaviors that complicate the optimization landscape of policy learning. Even further, generalizing to unseen embodiments demands that the policy captures meaningful shared control features that can be applied to novel physical embodiments.

Scaling hypothesis. We hypothesize that generalization improves with the number of training embodiments, i.e., larger $|\mathcal{E}_{\text{train}}|$ leads to higher J_{test}. Intuitively, training on more diverse embodiments encourages the policy to extract structural features that transfer to novel robots. For instance, despite differences in leg length or joint placement, many embodiments share similar locomotion dynamics and constraints. Discovering a scaling trend would provide empirical support for an embodiment scaling law and offer actionable insights for building general-purpose control policies.

Empirical setup. To study the hypothesis, we fix a constant test set by randomly holding out 20% of the generated embodiments. The remaining 80% serve as the pool for constructing training subsets $\mathcal{E}^{(i)}_{\text{train}} \subset \mathcal{E}_{\text{train}}$ at varying proportions $i \in (0, 1]$. For each subset, we train a separate policy $\pi^{(i)*}_{\text{train}}$ and evaluate it on the fixed $\mathcal{E}_{\text{test}}$. This setup enables a systematic analysis of generalization performance $J_{\text{test}}(\pi^{(i)*}_{\text{train}})$ as a function of training set size, probing for evidence of an embodiment scaling law.

Next, we describe how we generate diverse embodiments (Section 3.1), construct a policy to handle varying observation and action spaces (Section 3.2), and train it on many embodiments (Section 3.3).

3.1 Embodiment Generation

We adopt a procedural generation pipeline to produce diverse robot embodiments spanning three commonly used morphology classes: humanoid [41, 67, 90–94], quadruped [41, 55, 65, 73, 75, 95–99], and hexapod [41, 100–106]. Our generated robots follow common design patterns using realistic base components, such as link shapes, dimensions, and motor properties, but are procedurally composed into novel embodiments by varying their parameters. Geometric variation is introduced by scaling individual links and overall body size. Topological variation is achieved by changing the number of knee joints per leg within each morphology class. We also vary joint limits to implement

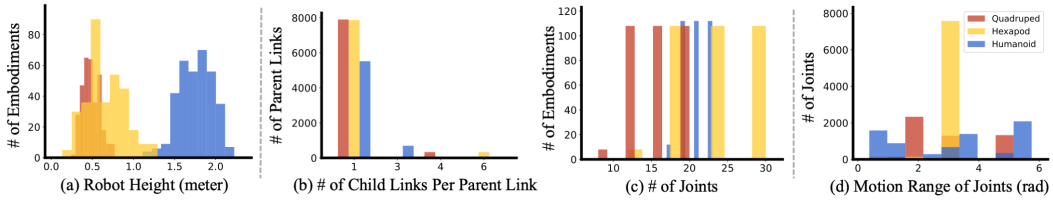

Figure 3: **Empirical distributions of embodiment variations in GENBOT-1K.** The statistics reflect geometric (a), topological (b,c), and kinematic (d) variability of embodiments in our dataset.

kinematic variations. In total, we generate 1,012 distinct robots, including 348 humanoids, 332 quadrupeds, and 332 hexapods, to form the GENBOT-1K dataset (Figure 1). Our resulting dataset is diverse in various aspects, as reflected in post-generation statistics (Figure 3). More details about the generation process are provided in Appendix B.

3.2 Cross-Embodiment Policy Architecture

To train a policy that can control $\sim$1000 different embodiments with different state and action spaces, we use URMA, an embodiment-aware architecture for robots with arbitrary numbers of joints [41]. URMA handles the differently sized partially observable states (observations) o of different embodiments by splitting them into fixed-length general observations o_g and varying-length joint-specific observations o_j, depending on the set of joints J of the current embodiment e (i.e., $o = (o_g, \{o_j\}_{j \in J})$). The embodiment descriptors $\phi(e)$ are used to generate joint description vectors d_j, which can uniquely describe every joint of the embodiment and are made up of the fixed dynamics and kinematics properties of the joint and its underlying motor. The joint-specific observations are processed by an attention encoder and are summed up into the joint latent vector

$$\bar{z}_{\text{joints}} = \sum_{j \in J} z_j, \qquad z_j = \frac{\exp\left(f_\phi(d_j)/\tau\right)}{\sum_{L_d} \exp\left(f_\phi(d_j)/\tau\right)} f_\psi(o_j), \tag{3}$$

where f_ϕ (with latent dimension L_d) and f_ψ are the encoders for the joint descriptions and joint observations, respectively, and τ is the learnable temperature parameter of the softmax. Intuitively, the attention mechanism fuses joint observations based on their descriptions so that $\bar{z}_{\text{joints}}$ has global information about the embodiment. The encoded joint latent vector is then concatenated with the general observations and processed by a core network to generate an action latent vector $\bar{z}_{\text{action}} = h_\theta(o_g, \bar{z}_{\text{joints}})$. To handle the differently sized action spaces, URMA concatenates the action latent vector with each encoded joint description vector in batch to decode a single action for each joint:

$$a_j = \mu_\nu(g_\omega(d_j), \bar{z}_{\text{action}}, z_j), \tag{4}$$

where g_ω is the action encoder for the joint descriptions, μ_ν is the final action decoder. In our work, we incorporate multi-head attention [107] into URMA, enabling the policy to attend to different joint-level features in parallel and better capture complex inter-joint dependencies (Appendix C.2).

3.3 Two-Stage Policy Learning

To scale cross-embodiment policy learning to a large number of robots, we adopt a two-stage paradigm. First, we train embodiment-specific expert policies using standard RL. Then, we collect demonstration data from these experts and train a single student policy via imitation learning, conditioned on embodiment descriptors. This approach allows learning across $\sim$1000 robots while maintaining tractable memory usage and stable training dynamics. The setup also mirrors real-world data pipelines, where large datasets are collected offline and reused across training runs (e.g., [21]).

Expert training. We develop a unified RL locomotion training pipeline applicable to all embodiments with minimal tuning. Key components include extensive domain randomization, performance-based curriculum learning, and regularization terms that encourage stable and natural locomotion (e.g., penalizing jittering movements and excessive ground contact). All robots in one morphology class share one set of hyperparameters for scalable training.

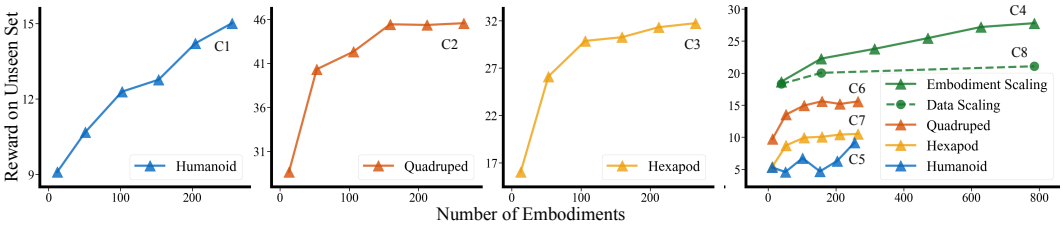

(a) Embodiment Scaling within Morphology Classes (b) Cross-Class Learning

Figure 4: **Results on embodiment scaling.** We evaluate generalization performance as a function of the number of training embodiments. (a) In-class study: policies are trained and tested within the same morphology class (humanoid, quadruped, or hexapod). (b) Cross-class study: We train policies on the full training set (green) and compare performance against policies trained on only the individual classes, while all policies are evaluated on the test set containing all classes. The proportion of training embodiments ($i \in \{0.05, 0.2, 0.4, 0.6, 0.8, 1.0\}$) is denoted in the x-axis. While the underlying reward function is the same, the reward scales differ across classes due to inherent differences in the embodiments (e.g., humanoids are less stable than quadrupeds) and unnormalized reward formulations (e.g., humanoids experience larger ground contact forces).

Training robust policies for ∼1,000 robot embodiments is computationally demanding. We use NVIDIA Isaac Lab [108] to train single-embodiment policies across 4,096 parallel environments with PPO [58]. Training all experts takes approximately 5 days on 160 NVIDIA RTX 4090/3090 GPUs, totaling over 2 trillion simulation steps. Full training details are provided in Appendix A.

Student distillation. Given expert policies $\{\pi_e\}_{e \in \mathcal{E}_{train}}$, we collect a demonstration dataset by rolling out each policy for 600 timesteps in 4,096 parallel environments, totaling 2 billion samples across all embodiments. We then train URMA by minimizing the Mean Squared Error (MSE):

$$\mathcal{L}_{\text{BC}} = \mathbb{E}_{(s_t, e, a_t) \sim \mathcal{D}} \left[\left\| \pi(s_t, \phi(e)) - a_t \right\|^2 \right], \tag{5}$$

where $\mathcal{D}$ is the expert demonstration dataset. The student policy conditions on the embodiment descriptor $\phi(e)$, enabling it to generalize across the generated embodiments with different geometry, topology, and kinematics. Training the model on the full demonstration dataset takes one week using a NVIDIA H100 GPU. More details about the distillation process can be found in Appendix C.

4 Experiments

In this section, we conduct a large-scale empirical study to investigate the scaling behavior of cross-embodiment learning. Our experiments are designed to answer the following key research questions:

- **Q1.** How does the generalization performance of the cross-embodiment policy scale with the number of training embodiments? (Sec. 4.1)
- **Q2.** Can the learned policy generalize zero-shot to unseen embodiments, including real-world robots, and handle varied kinematic constraints? (Sec. 4.2)
- **Q3.** Does the policy network learn meaningful, structured representations of the space of robot embodiments and morphologies through cross-embodiment training? (Sec. 4.3)

4.1 Studying Embodiment Scaling Laws

We train and evaluate our policies under multiple setups, with results illustrated in Figure 4. We analyze generalization patterns from three perspectives below. Additional results on out-of-distribution generalization are provided in Appendix D.

Scaling within each embodiment class. We conduct training and evaluation separately for each morphology class (humanoid, quadruped, and hexapod) in GenBot-1K, resulting in curves C1–C3. For each morphology class, we observe a clear scaling trend: increasing the number of training embodiments from 0.05 to 1.0 can double the cumulative reward. The rate of convergence varies by class: for quadrupeds and hexapods, performance saturates around 100 training embodiments, while for humanoids, it continues to improve steadily with more training data, likely due to greater

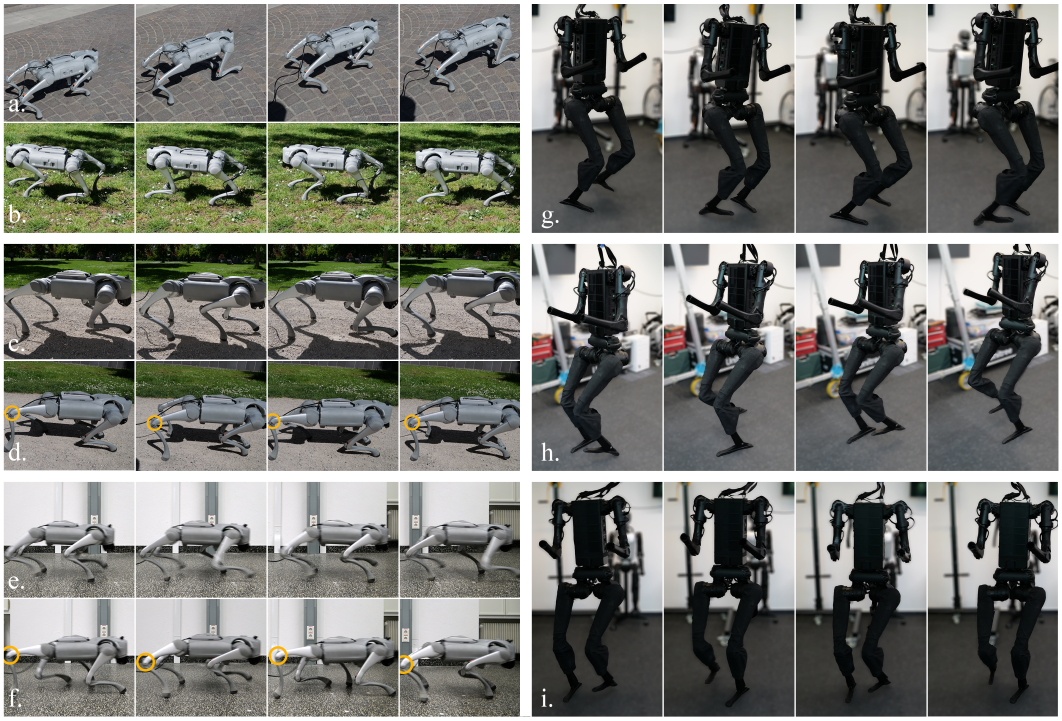

Figure 5: **Zero-shot generalization to unseen real-world robots.** Our URMA policy, trained on 817 diverse simulated embodiments, successfully transfers zero-shot to control the Unitree Go2 quadruped and Unitree H1 humanoid in the real world. **a, b:** The policy can perform forward and backward locomotion on cobblestone and grass terrain with the Go2. **c, d, e, f:** We test the policy's adaptation to kinematic constraints by artificially restricted the joint limits on the right rear knee of the Go2 by 20%. The policy effectively compensates for the limited range of motion, resulting in a stable limping gait on gravel (d) and indoors (f), compared to the unrestricted gait (c, e). **g, h:** Zero-shot transfer on the H1 works well in a lab environment, showing decent forward and backward locomotion. **i:** Walking side-to-side with H1 is slower as in simulation but stable in the real world.

instability and control difficulty. This suggests that more challenging embodiments may benefit more from larger-scale embodiment scaling.

Scaling across embodiment classes. We train on the full combined dataset of all three classes and evaluate on a unified test set (C4). The resulting curve begins at a reward of 18 and rises consistently to nearly 30, demonstrating that scaling across diverse embodiments enables broader generalization. We further evaluate the policies trained on individual morphology classes (corresponding to C1–C3) on the combined test set, obtaining (C5–C7). Since each of these models has only seen a single morphology class during training, their performance on the mixed test set is limited. In contrast, the best point on C4 achieves 2–5$\times$ higher average reward than C5–C7, demonstrating that training across diverse morphology classes enables substantially broader generalization.

Comparison with pure data scaling. To disentangle the effects of embodiment diversity from data quantity, we collect a dataset using only 5% of the training embodiments and vary the number of trajectories per embodiment for distillation (C8). We find that performance quickly saturates: the policy nearly reaches its peak at 0.2 data scale (4$\times$ data as 0.05), with negligible gains beyond that. This highlights that, if the goal is to achieve broad embodiment-level generalization, it is ineffective to only increase data volume on a small set of embodiments. Embodiment scaling is essential.

4.2 Real-World Generalization Test

To validate real-world transfer capabilities, we conducted zero-shot deployments of our best-performing policy, trained on the full training set of 817 simulated embodiments, on two real robots:

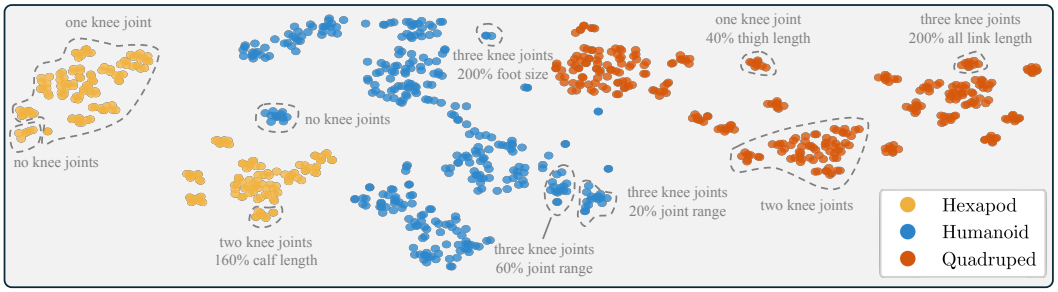

Figure 6: **Visualization of the embodiment latent space.** t-SNE projection of the action latent vectors on the complete GENBOT-1K dataset from the URMA policy trained on the full training set. Points are colored by morphology class. The clear clustering based on morphology class, and finer sub-structures related to the number of knee joints or kinematic and geometric properties, suggest that the policy learns a meaningful and structured representation of diverse embodiments, capturing functional similarities that help during cross-embodiment learning and enable generalization.

the Unitree Go2 quadruped and the Unitree H1 humanoid, neither of which was included in the training set $\mathcal{E}_{\text{train}}$, although robots with similar kinematic structures were present.

Figure 5 shows the policy successfully generalizing to the two real robots without any fine-tuning or modifications, using only the URDF of the respective robot to generate the embodiment descriptor $\phi(e)$. The Go2 demonstrated robust and stable walking gaits across diverse terrains such as grass, cobblestone, and gravel (a-c). Similarly, the H1 was able to maintain stable locomotion, tracking the desired velocity commands while walking on flat ground with rubber mats in a lab environment (g-i). While the transfer worked for both robots, the policy transferred worse to the H1 compared to the Go2, highlighting the need for potentially even more diverse humanoid robots in the training set.

To probe the policy's ability to handle kinematic variations in the real world, we artificially restricted the joint limits of the knee joints of the Go2 in 12 different configurations. We enforce different joint limits by pushing towards the artificial limits with high gains when the joint angles exceed them. Figure 5 (d, f) shows that the policy was able to transfer the adaptations it learned in simulation as it keeps the restricted rear right leg further back and maintains a stable limping gait.

4.3 Understanding Learned Embodiment Representations

To gain insight into the internal representations learned by our policy, we performed a t-distributed Stochastic Neighbor Embedding (t-SNE) [109] analysis on the action latent vectors $\bar{z}_{\text{action}}$ produced by URMA for each embodiment. Figure 6 shows that the learned representations naturally cluster according to the robot morphology, clearly distinguishing humanoids, quadrupeds, and hexapods. For all three morphologies, large clusters around the number of knee joints separate most of the latent space, showing the impact of additional joints on the policy. Many finer sub-clusters emerge based on different geometric and kinematic variations for a given number of knee joints. This structured representation indicates that our policy captures meaningful embodiment-specific features that generalize, mostly, within the morphology classes, whereas patterns across classes are less clear. Additional visualizations using PCA [110] and UMAP [111] can be found in Appendix F.

5 Conclusion

We conceptualize embodiment scaling laws and provide preliminary empirical evidence through a large-scale study on robot locomotion, using a procedurally generated dataset GENBOT-1K. Our results show that increasing the number of training embodiments improves generalization to unseen ones, with more challenging morphologies benefiting from continued scaling. Scaling across embodiment classes further enhances generalization, while simply increasing data volume on a fixed set of robots yields diminishing returns. We also demonstrate successful sim-to-real transfer of the learned cross-embodiment policy. As robotic platforms grow more diverse, the ability to learn from and generalize across embodiments becomes increasingly critical. We hope this work offers a step toward general-purpose cross-embodiment intelligence.

Limitations

While our work provides empirical evidence for embodiment scaling laws in robot learning, several limitations remain.

First, regarding task setup, our study focuses exclusively on locomotion on flat terrain for a highly controlled, foundational study. Extending this analysis to more complex tasks, such as vision-based manipulation or loco-manipulation, is an interesting exploration for future work.

Second, although our procedural generation pipeline produces a wide range of embodiments varying in topology, geometry, and joint constraints, it does not exhaustively cover the design space. Several factors, including body mass distribution, joint damping, and actuation type, are held fixed within a morphology class. Expanding the generation space to include such parameters could yield more robust generalization and offer further insights into the scaling behavior.

Finally, real-world experiments are limited to two physical robot platforms. Although we have modified their joint limits to create more kinematic variations, and existing results already demonstrated promising zero-shot transferability, broader validation on more diverse physical platforms, such as modular or reconfigurable robots, would provide stronger support for the generality of our findings.

Despite these limitations, we believe our study represents an important step toward understanding embodiment-level generalization and highlights the key role of embodiment scaling in the pursuit of generalizable robot learning.

Acknowledgments

This research is funded by the NSF AI-Center TILOS, the Hillbot Embodied AI Fund, the National Science Centre Poland (Weave programme UMO-2021/43/I/ST6/02711), and by the German Science Foundation (DFG) (grant number PE 2315/17-1).

Co-author Hao Su is the CTO for Hillbot and receives income. The terms of this arrangement have been reviewed and approved by the University of California, San Diego, in accordance with its conflict of interest policies.

We thank the German Research Center for AI (DFKI), Research Department: Systems AI for Robot Learning, for lending the Unitree Go2 and Unitree H1 robots.

Finally, we thank Oleg Kaidanov (DFKI, TU Darmstadt) for his continuous help with the real-world robot deployment, and we are grateful to the UCSD Su Lab members for facilitating extended access to compute resources, which made large-scale experiments feasible.

References

[1] A. Kirillov, E. Mintun, N. Ravi, H. Mao, C. Rolland, L. Gustafson, T. Xiao, S. Whitehead, A. C. Berg, W.-Y. Lo, P. Dollár, and R. Girshick. Segment anything. In *2023 IEEE/CVF International Conference on Computer Vision (ICCV)*, pages 3992–4003, 2023. doi:10.1109/ICCV51070.2023.00371.

[2] B. Wen, W. Yang, J. Kautz, and S. Birchfield. Foundationpose: Unified 6d pose estimation and tracking of novel objects. In *IEEE/CVF Conference on Computer Vision and Pattern Recognition, CVPR 2024, Seattle, WA, USA, June 16-22, 2024*, pages 17868–17879. IEEE, 2024. doi:10.1109/CVPR52733.2024.01692. URL `https://doi.org/10.1109/CVPR52733.2024.01692`.

[3] M. Caron, H. Touvron, I. Misra, H. Jégou, J. Mairal, P. Bojanowski, and A. Joulin. Emerging properties in self-supervised vision transformers. In *2021 IEEE/CVF International Conference on Computer Vision, ICCV 2021, Montreal, QC, Canada, October 10-17, 2021*, pages 9630–9640. IEEE, 2021. doi:10.1109/ICCV48922.2021.00951. URL `https://doi.org/10.1109/ICCV48922.2021.00951`.

[4] M. Oquab, T. Darcet, T. Moutakanni, H. V. Vo, M. Szafraniec, V. Khalidov, P. Fernandez, D. Haziza, F. Massa, A. El-Nouby, M. Assran, N. Ballas, W. Galuba, R. Howes, P. Huang, S. Li, I. Misra, M. Rabbat, V. Sharma, G. Synnaeve, H. Xu, H. Jégou, J. Mairal, P. Labatut, A. Joulin, and P. Bojanowski. Dinov2: Learning robust visual features without supervision. *Trans. Mach. Learn. Res.*, 2024, 2024. URL https://openreview.net/forum?id=a68SUt6zFt.

[5] X. Zhai, A. Kolesnikov, N. Houlsby, and L. Beyer. Scaling vision transformers. In *IEEE/CVF Conference on Computer Vision and Pattern Recognition, CVPR 2022, New Orleans, LA, USA, June 18-24, 2022*, pages 1204–1213. IEEE, 2022. doi:10.1109/CVPR52688.2022.01179. URL https://doi.org/10.1109/CVPR52688.2022.01179.

[6] C. Sun, A. Shrivastava, S. Singh, and A. Gupta. Revisiting unreasonable effectiveness of data in deep learning era. In *IEEE International Conference on Computer Vision, ICCV 2017, Venice, Italy, October 22-29, 2017*, pages 843–852. IEEE Computer Society, 2017. doi:10.1109/ICCV.2017.97. URL https://doi.org/10.1109/ICCV.2017.97.

[7] T. Tian, H. Li, B. Ai, X. Yuan, Z. Huang, and H. Su. Diffusion dynamics models with generative state estimation for cloth manipulation. *CoRR*, abs/2503.11999, 2025. doi:10.48550/ARXIV.2503.11999. URL https://doi.org/10.48550/arXiv.2503.11999.

[8] D. Mahajan, R. B. Girshick, V. Ramanathan, K. He, M. Paluri, Y. Li, A. Bharambe, and L. van der Maaten. Exploring the limits of weakly supervised pretraining. In V. Ferrari, M. Hebert, C. Sminchisescu, and Y. Weiss, editors, *Computer Vision - ECCV 2018 - 15th European Conference, Munich, Germany, September 8-14, 2018, Proceedings, Part II*, volume 11206 of *Lecture Notes in Computer Science*, pages 185–201. Springer, 2018. doi:10.1007/978-3-030-01216-8_12. URL https://doi.org/10.1007/978-3-030-01216-8_12.

[9] L. Ouyang, J. Wu, X. Jiang, D. Almeida, C. L. Wainwright, P. Mishkin, C. Zhang, S. Agarwal, K. Slama, A. Ray, J. Schulman, J. Hilton, F. Kelton, L. Miller, M. Simens, A. Askell, P. Welinder, P. F. Christiano, J. Leike, and R. Lowe. Training language models to follow instructions with human feedback. In S. Koyejo, S. Mohamed, A. Agarwal, D. Belgrave, K. Cho, and A. Oh, editors, *Advances in Neural Information Processing Systems 35: Annual Conference on Neural Information Processing Systems 2022, NeurIPS 2022, New Orleans, LA, USA, November 28 - December 9, 2022*, 2022. URL http://papers.nips.cc/paper_files/paper/2022/hash/b1efde53be364a73914f58805a001731-Abstract-Conference.html.

[10] J. Achiam, S. Adler, S. Agarwal, L. Ahmad, I. Akkaya, F. L. Aleman, D. Almeida, J. Altenschmidt, S. Altman, S. Anadkat, et al. Gpt-4 technical report. *arXiv preprint arXiv:2303.08774*, 2023.

[11] DeepSeek-AI, D. Guo, D. Yang, H. Zhang, J. Song, R. Zhang, R. Xu, Q. Zhu, S. Ma, P. Wang, X. Bi, X. Zhang, X. Yu, Y. Wu, Z. F. Wu, Z. Gou, Z. Shao, Z. Li, Z. Gao, A. Liu, B. Xue, B. Wang, B. Wu, B. Feng, C. Lu, C. Zhao, C. Deng, C. Zhang, C. Ruan, D. Dai, D. Chen, D. Ji, E. Li, F. Lin, F. Dai, F. Luo, G. Hao, G. Chen, G. Li, H. Zhang, H. Bao, H. Xu, H. Wang, H. Ding, H. Xin, H. Gao, H. Qu, H. Li, J. Guo, J. Li, J. Wang, J. Chen, J. Yuan, J. Qiu, J. Li, J. L. Cai, J. Ni, J. Liang, J. Chen, K. Dong, K. Hu, K. Gao, K. Guan, K. Huang, K. Yu, L. Wang, L. Zhang, L. Zhao, L. Wang, L. Zhang, L. Xu, L. Xia, M. Zhang, M. Zhang, M. Tang, M. Li, M. Wang, M. Li, N. Tian, P. Huang, P. Zhang, Q. Wang, Q. Chen, Q. Du, R. Ge, R. Zhang, R. Pan, R. Wang, R. J. Chen, R. L. Jin, R. Chen, S. Lu, S. Zhou, S. Chen, S. Ye, S. Wang, S. Yu, S. Zhou, S. Pan, S. S. Li, S. Zhou, S. Wu, S. Ye, T. Yun, T. Pei, T. Sun, T. Wang, W. Zeng, W. Zhao, W. Liu, W. Liang, W. Gao, W. Yu, W. Zhang, W. L. Xiao, W. An, X. Liu, X. Wang, X. Chen, X. Nie, X. Cheng, X. Liu, X. Xie, X. Liu, X. Yang, X. Li, X. Su, X. Lin, X. Q. Li, X. Jin, X. Shen, X. Chen, X. Sun, X. Wang, X. Song, X. Zhou, X. Wang, X. Shan, Y. K. Li, Y. Q. Wang, Y. X. Wei, Y. Zhang, Y. Xu, Y. Li, Y. Zhao, Y. Sun, Y. Wang, Y. Yu, Y. Zhang, Y. Shi, Y. Xiong, Y. He, Y. Piao, Y. Wang, Y. Tan, Y. Ma, Y. Liu,

Y. Guo, Y. Ou, Y. Wang, Y. Gong, Y. Zou, Y. He, Y. Xiong, Y. Luo, Y. You, Y. Liu, Y. Zhou, Y. X. Zhu, Y. Xu, Y. Huang, Y. Li, Y. Zheng, Y. Zhu, Y. Ma, Y. Tang, Y. Zha, Y. Yan, Z. Z. Ren, Z. Ren, Z. Sha, Z. Fu, Z. Xu, Z. Xie, Z. Zhang, Z. Hao, Z. Ma, Z. Yan, Z. Wu, Z. Gu, Z. Zhu, Z. Liu, Z. Li, Z. Xie, Z. Song, Z. Pan, Z. Huang, Z. Xu, Z. Zhang, and Z. Zhang. Deepseek-r1: Incentivizing reasoning capability in llms via reinforcement learning, 2025. URL https://arxiv.org/abs/2501.12948.

[12] J. Kaplan, S. McCandlish, T. Henighan, T. B. Brown, B. Chess, R. Child, S. Gray, A. Radford, J. Wu, and D. Amodei. Scaling laws for neural language models. *CoRR*, abs/2001.08361, 2020. URL https://arxiv.org/abs/2001.08361.

[13] A. Chowdhery, S. Narang, J. Devlin, M. Bosma, G. Mishra, A. Roberts, P. Barham, H. W. Chung, C. Sutton, S. Gehrmann, P. Schuh, K. Shi, S. Tsvyashchenko, J. Maynez, A. Rao, P. Barnes, Y. Tay, N. Shazeer, V. Prabhakaran, E. Reif, N. Du, B. Hutchinson, R. Pope, J. Bradbury, J. Austin, M. Isard, G. Gur-Ari, P. Yin, T. Duke, A. Levskaya, S. Ghemawat, S. Dev, H. Michalewski, X. Garcia, V. Misra, K. Robinson, L. Fedus, D. Zhou, D. Ippolito, D. Luan, H. Lim, B. Zoph, A. Spiridonov, R. Sepassi, D. Dohan, S. Agrawal, M. Omernick, A. M. Dai, T. S. Pillai, M. Pellat, A. Lewkowycz, E. Moreira, R. Child, O. Polozov, K. Lee, Z. Zhou, X. Wang, B. Saeta, M. Diaz, O. Firat, M. Catasta, J. Wei, K. Meier-Hellstern, D. Eck, J. Dean, S. Petrov, and N. Fiedel. Palm: Scaling language modeling with pathways, 2022. URL https://arxiv.org/abs/2204.02311.

[14] T. Gao, A. Fisch, and D. Chen. Making pre-trained language models better few-shot learners. In C. Zong, F. Xia, W. Li, and R. Navigli, editors, *Proceedings of the 59th Annual Meeting of the Association for Computational Linguistics and the 11th International Joint Conference on Natural Language Processing (Volume 1: Long Papers)*, pages 3816–3830, Online, Aug. 2021. Association for Computational Linguistics. doi:10.18653/v1/2021.acl-long.295. URL https://aclanthology.org/2021.acl-long.295/.

[15] J. Hoffmann, S. Borgeaud, A. Mensch, E. Buchatskaya, T. Cai, E. Rutherford, D. de Las Casas, L. A. Hendricks, J. Welbl, A. Clark, T. Hennigan, E. Noland, K. Millican, G. van den Driessche, B. Damoc, A. Guy, S. Osindero, K. Simonyan, E. Elsen, J. W. Rae, O. Vinyals, and L. Sifre. Training compute-optimal large language models. *CoRR*, abs/2203.15556, 2022. doi:10.48550/ARXIV.2203.15556. URL https://doi.org/10.48550/arXiv.2203.15556.

[16] B. Ai, Y. Wang, Y. Tan, and S. Tan. Whodunit? learning to contrast for authorship attribution. In Y. He, H. Ji, Y. Liu, S. Li, C. Chang, S. Poria, C. Lin, W. L. Buntine, M. Liakata, H. Yan, Z. Yan, S. Ruder, X. Wan, M. Arana-Catania, Z. Wei, H. Huang, J. Wu, M. Day, P. Liu, and R. Xu, editors, *Proceedings of the 2nd Conference of the Asia-Pacific Chapter of the Association for Computational Linguistics and the 12th International Joint Conference on Natural Language Processing, AACL/IJCNLP 2022 - Volume 1: Long Papers, Online Only, November 20-23, 2022*, pages 1142–1157. Association for Computational Linguistics, 2022. URL https://aclanthology.org/2022.aacl-main.84.

[17] Z. Wu, B. Ai, and D. Hsu. Integrating common sense and planning with large language models for room tidying. In *RSS 2023 Workshop on Learning for Task and Motion Planning*, 2023. URL https://openreview.net/forum?id=vuSI9mhDaBZ.

[18] Q. Gao, X. Pi, K. Liu, J. Chen, R. Yang, X. Huang, X. Fang, L. Sun, G. Kishore, B. Ai, S. Tao, M. Liu, J. Yang, C.-J. Lai, C. Jin, J. Xiang, B. Huang, D. Danks, H. Su, T. Shu, Z. Ma, L. Qin, and Z. Hu. Do vision-language models have internal world models? towards an atomic evaluation. In *ICLR 2025 Workshop on World Models: Understanding, Modelling and Scaling*, 2025. URL https://openreview.net/forum?id=tpPv3ayoqo.

[19] K. Fang, P. Yin, A. Nair, H. Walke, G. Yan, and S. Levine. Generalization with lossy affordances: Leveraging broad offline data for learning visuomotor tasks. In K. Liu, D. Kulic, and

J. Ichnowski, editors, *Conference on Robot Learning, CoRL 2022, 14-18 December 2022, Auckland, New Zealand*, volume 205 of *Proceedings of Machine Learning Research*, pages 106–117. PMLR, 2022. URL https://proceedings.mlr.press/v205/fang23a.html.

[20] A. Kumar, A. Singh, F. D. Ebert, M. Nakamoto, Y. Yang, C. Finn, and S. Levine. Pre-training for robots: Offline RL enables learning new tasks in a handful of trials. In K. E. Bekris, K. Hauser, S. L. Herbert, and J. Yu, editors, *Robotics: Science and Systems XIX, Daegu, Republic of Korea, July 10-14, 2023*, 2023. doi:10.15607/RSS.2023.XIX.019. URL https://doi.org/10.15607/RSS.2023.XIX.019.

[21] A. O'Neill, A. Rehman, A. Maddukuri, A. Gupta, A. Padalkar, A. Lee, A. Pooley, A. Gupta, A. Mandlekar, A. Jain, A. Tung, A. Bewley, A. Herzog, A. Irpan, A. Khazatsky, A. Rai, A. Gupta, A. Wang, A. Singh, A. Garg, A. Kembhavi, A. Xie, A. Brohan, A. Raffin, A. Sharma, A. Yavary, A. Jain, A. Balakrishna, A. Wahid, B. Burgess-Limerick, B. Kim, B. Schölkopf, B. Wulfe, B. Ichter, C. Lu, C. Xu, C. Le, C. Finn, C. Wang, C. Xu, C. Chi, C. Huang, C. Chan, C. Agia, C. Pan, C. Fu, C. Devin, D. Xu, D. Morton, D. Driess, D. Chen, D. Pathak, D. Shah, D. Büchler, D. Jayaraman, D. Kalashnikov, D. Sadigh, E. Johns, E. P. Foster, F. Liu, F. Ceola, F. Xia, F. Zhao, F. Stulp, G. Zhou, G. S. Sukhatme, G. Salhotra, G. Yan, G. Feng, G. Schiavi, G. Berseth, G. Kahn, G. Wang, H. Su, H. Fang, H. Shi, H. Bao, H. B. Amor, H. I. Christensen, H. Furuta, H. Walke, H. Fang, H. Ha, I. Mordatch, I. Radosavovic, I. Leal, J. Liang, J. Abou-Chakra, J. Kim, J. Drake, J. Peters, J. Schneider, J. Hsu, J. Bohg, J. Bingham, J. Wu, J. Gao, J. Hu, J. Wu, J. Wu, J. Sun, J. Luo, J. Gu, J. Tan, J. Oh, J. Wu, J. Lu, J. Yang, J. Malik, J. Silvério, J. Hejna, J. Booher, J. Tompson, J. Yang, J. Salvador, J. J. Lim, J. Han, K. Wang, K. Rao, K. Pertsch, K. Hausman, K. Go, K. Gopalakrishnan, K. Goldberg, K. Byrne, K. Oslund, K. Kawaharazuka, K. Black, K. Lin, K. Zhang, K. Ehsani, K. Lekkala, K. Ellis, K. Rana, K. Srinivasan, K. Fang, K. P. Singh, K. Zeng, K. Hatch, K. Hsu, L. Itti, L. Y. Chen, L. Pinto, L. Fei-Fei, L. Tan, L. J. Fan, L. Ott, L. Lee, L. Weihs, M. Chen, M. Lepert, M. Memmel, M. Tomizuka, M. Itkina, M. G. Castro, M. Spero, M. Du, M. Ahn, M. C. Yip, M. Zhang, M. Ding, M. Heo, M. K. Srirama, M. Sharma, M. J. Kim, N. Kanazawa, N. Hansen, N. Heess, N. J. Joshi, N. Sünderhauf, N. Liu, N. D. Palo, N. M. M. Shafiullah, O. Mees, O. Kroemer, O. Bastani, P. R. Sanketi, P. T. Miller, P. Yin, P. Wohlhart, P. Xu, P. D. Fagan, P. Mitrano, P. Sermanet, P. Abbeel, P. Sundaresan, Q. Chen, Q. Vuong, R. Rafailov, R. Tian, R. Doshi, R. Martín-Martín, R. Baijal, R. Scalise, R. Hendrix, R. Lin, R. Qian, R. Zhang, R. Mendonca, R. Shah, R. Hoque, R. Julian, S. Bustamante, S. Kirmani, S. Levine, S. Lin, S. Moore, S. Bahl, S. Dass, S. D. Sonawani, S. Song, S. Xu, S. Haldar, S. Karamcheti, S. Adebola, S. Guist, S. Nasiriany, S. Schaal, S. Welker, S. Tian, S. Ramamoorthy, S. Dasari, S. Belkhale, S. Park, S. Nair, S. Mirchandani, T. Osa, T. Gupta, T. Harada, T. Matsushima, T. Xiao, T. Kollar, T. Yu, T. Ding, T. Davchev, T. Z. Zhao, T. Armstrong, T. Darrell, T. Chung, V. Jain, V. Vanhoucke, W. Zhan, W. Zhou, W. Burgard, X. Chen, X. Wang, X. Zhu, X. Geng, X. Liu, L. Xu, X. Li, Y. Lu, Y. J. Ma, Y. Kim, Y. Chebotar, Y. Zhou, Y. Zhu, Y. Wu, Y. Xu, Y. Wang, Y. Bisk, Y. Cho, Y. Lee, Y. Cui, Y. Cao, Y. Wu, Y. Tang, Y. Zhu, Y. Zhang, Y. Jiang, Y. Li, Y. Li, Y. Iwasawa, Y. Matsuo, Z. Ma, Z. Xu, Z. J. Cui, Z. Zhang, and Z. Lin. Open x-embodiment: Robotic learning datasets and RT-X models : Open x-embodiment collaboration. In *IEEE International Conference on Robotics and Automation, ICRA 2024, Yokohama, Japan, May 13-17, 2024*, pages 6892–6903. IEEE, 2024. doi:10.1109/ICRA57147.2024.10611477. URL https://doi.org/10.1109/ICRA57147.2024.10611477.

[22] D. Ghosh, H. R. Walke, K. Pertsch, K. Black, O. Mees, S. Dasari, J. Hejna, T. Kreiman, C. Xu, J. Luo, Y. L. Tan, L. Y. Chen, Q. Vuong, T. Xiao, P. R. Sanketi, D. Sadigh, C. Finn, and S. Levine. Octo: An open-source generalist robot policy. In D. Kulic, G. Venture, K. E. Bekris, and E. Coronado, editors, *Robotics: Science and Systems XX, Delft, The Netherlands, July 15-19, 2024*, 2024. doi:10.15607/RSS.2024.XX.090. URL https://doi.org/10.15607/RSS.2024.XX.090.

[23] A. Brohan, N. Brown, J. Carbajal, Y. Chebotar, J. Dabis, C. Finn, K. Gopalakrishnan, K. Hausman, A. Herzog, J. Hsu, J. Ibarz, B. Ichter, A. Irpan, T. Jackson, S. Jesmonth, N. J. Joshi, R. Julian, D. Kalashnikov, Y. Kuang, I. Leal, K. Lee, S. Levine, Y. Lu, U. Malla, D. Manjunath, I. Mordatch, O. Nachum, C. Parada, J. Peralta, E. Perez, K. Pertsch, J. Quiambao, K. Rao, M. S. Ryoo, G. Salazar, P. R. Sanketi, K. Sayed, J. Singh, S. Sontakke, A. Stone, C. Tan, H. T. Tran, V. Vanhoucke, S. Vega, Q. Vuong, F. Xia, T. Xiao, P. Xu, S. Xu, T. Yu, and B. Zitkovich. RT-1: robotics transformer for real-world control at scale. In K. E. Bekris, K. Hauser, S. L. Herbert, and J. Yu, editors, *Robotics: Science and Systems XIX, Daegu, Republic of Korea, July 10-14, 2023*, 2023. doi:10.15607/RSS.2023.XIX.025. URL https://doi.org/10.15607/RSS.2023.XIX.025.

[24] B. Zitkovich, T. Yu, S. Xu, P. Xu, T. Xiao, F. Xia, J. Wu, P. Wohlhart, S. Welker, A. Wahid, Q. Vuong, V. Vanhoucke, H. T. Tran, R. Soricut, A. Singh, J. Singh, P. Sermanet, P. R. Sanketi, G. Salazar, M. S. Ryoo, K. Reymann, K. Rao, K. Pertsch, I. Mordatch, H. Michalewski, Y. Lu, S. Levine, L. Lee, T. E. Lee, I. Leal, Y. Kuang, D. Kalashnikov, R. Julian, N. J. Joshi, A. Irpan, B. Ichter, J. Hsu, A. Herzog, K. Hausman, K. Gopalakrishnan, C. Fu, P. Florence, C. Finn, K. A. Dubey, D. Driess, T. Ding, K. M. Choromanski, X. Chen, Y. Chebotar, J. Carbajal, N. Brown, A. Brohan, M. G. Arenas, and K. Han. RT-2: vision-language-action models transfer web knowledge to robotic control. In J. Tan, M. Toussaint, and K. Darvish, editors, *Conference on Robot Learning, CoRL 2023, 6-9 November 2023, Atlanta, GA, USA*, volume 229 of *Proceedings of Machine Learning Research*, pages 2165–2183. PMLR, 2023. URL https://proceedings.mlr.press/v229/zitkovich23a.html.

[25] P. Intelligence, K. Black, N. Brown, J. Darpinian, K. Dhabalia, D. Driess, A. Esmail, M. Equi, C. Finn, N. Fusai, M. Y. Galliker, D. Ghosh, L. Groom, K. Hausman, B. Ichter, S. Jakubczak, T. Jones, L. Ke, D. LeBlanc, S. Levine, A. Li-Bell, M. Mothukuri, S. Nair, K. Pertsch, A. Z. Ren, L. X. Shi, L. Smith, J. T. Springenberg, K. Stachowicz, J. Tanner, Q. Vuong, H. Walke, A. Walling, H. Wang, L. Yu, and U. Zhilinsky. $\pi_{0.5}$: a vision-language-action model with open-world generalization, 2025. URL https://arxiv.org/abs/2504.16054.

[26] H. Fang, H. Fang, Z. Tang, J. Liu, C. Wang, J. Wang, H. Zhu, and C. Lu. RH20T: A comprehensive robotic dataset for learning diverse skills in one-shot. In *IEEE International Conference on Robotics and Automation, ICRA 2024, Yokohama, Japan, May 13-17, 2024*, pages 653–660. IEEE, 2024. doi:10.1109/ICRA57147.2024.10611615. URL https://doi.org/10.1109/ICRA57147.2024.10611615.

[27] M. J. Kim, K. Pertsch, S. Karamcheti, T. Xiao, A. Balakrishna, S. Nair, R. Rafailov, E. P. Foster, P. R. Sanketi, Q. Vuong, T. Kollar, B. Burchfiel, R. Tedrake, D. Sadigh, S. Levine, P. Liang, and C. Finn. Openvla: An open-source vision-language-action model. In P. Agrawal, O. Kroemer, and W. Burgard, editors, *Conference on Robot Learning, 6-9 November 2024, Munich, Germany*, volume 270 of *Proceedings of Machine Learning Research*, pages 2679–2713. PMLR, 2024. URL https://proceedings.mlr.press/v270/kim25c.html.

[28] K. Black, N. Brown, D. Driess, A. Esmail, M. Equi, C. Finn, N. Fusai, L. Groom, K. Hausman, B. Ichter, et al. π0: A vision-language-action flow model for general robot control, 2024. *URL https://arxiv. org/abs/2410.24164*, 2025.

[29] F. Ebert, Y. Yang, K. Schmeckpeper, B. Bucher, G. Georgakis, K. Daniilidis, C. Finn, and S. Levine. Bridge data: Boosting generalization of robotic skills with cross-domain datasets. In K. Hauser, D. A. Shell, and S. Huang, editors, *Robotics: Science and Systems XVIII, New York City, NY, USA, June 27 - July 1, 2022*, 2022. doi:10.15607/RSS.2022.XVIII.063. URL https://doi.org/10.15607/RSS.2022.XVIII.063.

[30] H. R. Walke, K. Black, T. Z. Zhao, Q. Vuong, C. Zheng, P. Hansen-Estruch, A. W. He, V. Myers, M. J. Kim, M. Du, A. Lee, K. Fang, C. Finn, and S. Levine. Bridgedata V2: A dataset for robot learning at scale. In J. Tan, M. Toussaint, and K. Darvish, editors, *Conference on Robot Learning, CoRL 2023, 6-9 November 2023, Atlanta, GA, USA*, volume 229 of

Proceedings of Machine Learning Research, pages 1723–1736. PMLR, 2023. URL https://proceedings.mlr.press/v229/walke23a.html.

[31] F. Lin, Y. Hu, P. Sheng, C. Wen, J. You, and Y. Gao. Data scaling laws in imitation learning for robotic manipulation. *CoRR*, abs/2410.18647, 2024. doi:10.48550/ARXIV.2410.18647. URL https://doi.org/10.48550/arXiv.2410.18647.

[32] H. Fang, C. Wang, M. Gou, and C. Lu. Graspnet-1billion: A large-scale benchmark for general object grasping. In *2020 IEEE/CVF Conference on Computer Vision and Pattern Recognition, CVPR 2020, Seattle, WA, USA, June 13-19, 2020*, pages 11441–11450. Computer Vision Foundation / IEEE, 2020. doi:10.1109/CVPR42600.2020.01146. URL https://openaccess.thecvf.com/content_CVPR_2020/html/Fang_GraspNet-1Billion_A_Large-Scale_Benchmark_for_General_Object_Grasping_CVPR_2020_paper.html.

[33] W. Gao, B. Ai, J. Loo, Vinay, and D. Hsu. Intentionnet: Map-lite visual navigation at the kilometre scale, 2024. URL https://arxiv.org/abs/2407.03122.

[34] B. Ai, Z. Wu, and D. Hsu. Invariance is key to generalization: Examining the role of representation in sim-to-real transfer for visual navigation. In M. H. Ang Jr and O. Khatib, editors, *Experimental Robotics*, pages 69–80, Cham, 2024. Springer Nature Switzerland. ISBN 978-3-031-63596-0.

[35] B. Ai, W. Gao, Vinay, and D. Hsu. Deep visual navigation under partial observability. In *2022 International Conference on Robotics and Automation, ICRA 2022, Philadelphia, PA, USA, May 23-27, 2022*, pages 9439–9446. IEEE, 2022. doi:10.1109/ICRA46639.2022.9811598. URL https://doi.org/10.1109/ICRA46639.2022.9811598.

[36] N. M. M. Shafiullah, A. Rai, H. Etukuru, Y. Liu, I. Misra, S. Chintala, and L. Pinto. On bringing robots home. *arXiv preprint arXiv:2311.16098*, 2023.

[37] A. Mandlekar, S. Nasiriany, B. Wen, I. Akinola, Y. S. Narang, L. Fan, Y. Zhu, and D. Fox. Mimicgen: A data generation system for scalable robot learning using human demonstrations. In J. Tan, M. Toussaint, and K. Darvish, editors, *Conference on Robot Learning, CoRL 2023, 6-9 November 2023, Atlanta, GA, USA*, volume 229 of *Proceedings of Machine Learning Research*, pages 1820–1864. PMLR, 2023. URL https://proceedings.mlr.press/v229/mandlekar23a.html.

[38] S. Dasari, F. Ebert, S. Tian, S. Nair, B. Bucher, K. Schmeckpeper, S. Singh, S. Levine, and C. Finn. Robonet: Large-scale multi-robot learning. In L. P. Kaelbling, D. Kragic, and K. Sugiura, editors, *3rd Annual Conference on Robot Learning, CoRL 2019, Osaka, Japan, October 30 - November 1, 2019, Proceedings*, volume 100 of *Proceedings of Machine Learning Research*, pages 885–897. PMLR, 2019. URL http://proceedings.mlr.press/v100/dasari20a.html.

[39] A. Khazatsky, K. Pertsch, S. Nair, A. Balakrishna, S. Dasari, S. Karamcheti, S. Nasiriany, M. K. Srirama, L. Y. Chen, K. Ellis, P. D. Fagan, J. Hejna, M. Itkina, M. Lepert, Y. J. Ma, P. T. Miller, J. Wu, S. Belkhale, S. Dass, H. Ha, A. Jain, A. Lee, Y. Lee, M. Memmel, S. Park, I. Radosavovic, K. Wang, A. Zhan, K. Black, C. Chi, K. B. Hatch, S. Lin, J. Lu, J. Mercat, A. Rehman, P. R. Sanketi, A. Sharma, C. Simpson, Q. Vuong, H. R. Walke, B. Wulfe, T. Xiao, J. H. Yang, A. Yavary, T. Z. Zhao, C. Agia, R. Baijal, M. G. Castro, D. Chen, Q. Chen, T. Chung, J. Drake, E. P. Foster, J. Gao, D. A. Herrera, M. Heo, K. Hsu, J. Hu, D. Jackson, C. Le, Y. Li, R. Lin, Z. Ma, A. Maddukuri, S. Mirchandani, D. Morton, T. Nguyen, A. O'Neill, R. Scalise, D. Seale, V. Son, S. Tian, E. Tran, A. E. Wang, Y. Wu, A. Xie, J. Yang, P. Yin, Y. Zhang, O. Bastani, G. Berseth, J. Bohg, K. Goldberg, A. Gupta, A. Gupta, D. Jayaraman, J. J. Lim, J. Malik, R. Martín-Martín, S. Ramamoorthy, D. Sadigh, S. Song, J. Wu, M. C. Yip, Y. Zhu, T. Kollar, S. Levine, and C. Finn. DROID: A large-scale in-the-wild robot manipulation dataset. In D. Kulic, G. Venture, K. E. Bekris, and E. Coronado,

editors, *Robotics: Science and Systems XX, Delft, The Netherlands, July 15-19, 2024*, 2024. doi:10.15607/RSS.2024.XX.120. URL https://doi.org/10.15607/RSS.2024.XX.120.

[40] A. Patel and S. Song. Get-zero: Graph embodiment transformer for zero-shot embodiment generalization. *CoRR*, abs/2407.15002, 2024. doi:10.48550/ARXIV.2407.15002. URL https://doi.org/10.48550/arXiv.2407.15002.

[41] N. Bohlinger, G. Czechmanowski, M. Krupka, P. Kicki, K. Walas, J. Peters, and D. Tateo. One policy to run them all: an end-to-end learning approach to multi-embodiment locomotion. *Conference on Robot Learning*, 2024.

[42] Z. Jia, X. Li, Z. Ling, S. Liu, Y. Wu, and H. Su. Improving policy optimization with generalist-specialist learning. In K. Chaudhuri, S. Jegelka, L. Song, C. Szepesvári, G. Niu, and S. Sabato, editors, *International Conference on Machine Learning, ICML 2022, 17-23 July 2022, Baltimore, Maryland, USA*, volume 162 of *Proceedings of Machine Learning Research*, pages 10104–10119. PMLR, 2022. URL https://proceedings.mlr.press/v162/jia22a.html.

[43] W. Wan, H. Geng, Y. Liu, Z. Shan, Y. Yang, L. Yi, and H. Wang. Unidexgrasp++: Improving dexterous grasping policy learning via geometry-aware curriculum and iterative generalist-specialist learning. In *IEEE/CVF International Conference on Computer Vision, ICCV 2023, Paris, France, October 1-6, 2023*, pages 3868–3879. IEEE, 2023. doi:10.1109/ICCV51070.2023.00360. URL https://doi.org/10.1109/ICCV51070.2023.00360.

[44] R. Zhu, T. Dai, and O. Celiktutan. Cross domain policy transfer with effect cycle-consistency. In *2024 IEEE International Conference on Robotics and Automation*. IEEE Explore, 2024.

[45] Y. Chen, Y. Chen, Z. Hu, T. Yang, C. Fan, Y. Yu, and J. Hao. Learning action-transferable policy with action embedding. *arXiv preprint arXiv:1909.02291*, 2019.

[46] Y. Hu and G. Montana. Skill transfer in deep reinforcement learning under morphological heterogeneity. *arXiv preprint arXiv:1908.05265*, 2019.

[47] X. Liu, D. Pathak, and D. Zhao. Meta-evolve: Continuous robot evolution for one-to-many policy transfer. In *The Twelfth International Conference on Learning Representations*, 2024.

[48] T. Wang, R. Liao, J. Ba, and S. Fidler. Nervenet: Learning structured policy with graph neural networks. In *International Conference on Learning Representations*, 2018.

[49] W. Huang, I. Mordatch, and D. Pathak. One policy to control them all: Shared modular policies for agent-agnostic control. In *Proceedings of the 37th International Conference on Machine Learning, ICML 2020, 13-18 July 2020, Virtual Event*, volume 119 of *Proceedings of Machine Learning Research*, pages 4455–4464. PMLR, 2020. URL http://proceedings.mlr.press/v119/huang20d.html.

[50] B. Trabucco, M. Phielipp, and G. Berseth. Anymorph: Learning transferable polices by inferring agent morphology. In *International Conference on Machine Learning*, pages 21677–21691. PMLR, 2022.

[51] H. Furuta, Y. Iwasawa, Y. Matsuo, and S. S. Gu. A system for morphology-task generalization via unified representation and behavior distillation. In *The Eleventh International Conference on Learning Representations*, 2022.

[52] D. Shah, A. Sridhar, A. Bhorkar, N. Hirose, and S. Levine. Gnm: A general navigation model to drive any robot. In *2023 IEEE International Conference on Robotics and Automation (ICRA)*, pages 7226–7233. IEEE, 2023.

[53] W. Song, H. Zhao, P. Ding, C. Cui, S. Lyu, Y. Fan, and D. Wang. Germ: A generalist robotic model with mixture-of-experts for quadruped robot. *arXiv preprint arXiv:2403.13358*, 2024.

[54] R. Doshi, H. R. Walke, O. Mees, S. Dasari, and S. Levine. Scaling cross-embodied learning: One policy for manipulation, navigation, locomotion and aviation. In *8th Annual Conference on Robot Learning*, 2024.

[55] M. Shafiee, G. Bellegarda, and A. Ijspeert. Manyquadrupeds: Learning a single locomotion policy for diverse quadruped robots. In *2024 IEEE International Conference on Robotics and Automation (ICRA)*, pages 3471–3477. IEEE, 2024.

[56] A. Eftekhar, L. Weihs, R. Hendrix, E. Caglar, J. Salvador, A. Herrasti, W. Han, E. VanderBil, A. Kembhavi, A. Farhadi, et al. The one ring: a robotic indoor navigation generalist. *arXiv preprint arXiv:2412.14401*, 2024.

[57] G. Feng, H. Zhang, Z. Li, X. B. Peng, B. Basireddy, L. Yue, Z. Song, L. Yang, Y. Liu, K. Sreenath, and S. Levine. Genloco: Generalized locomotion controllers for quadrupedal robots. In K. Liu, D. Kulic, and J. Ichnowski, editors, *Conference on Robot Learning, CoRL 2022, 14-18 December 2022, Auckland, New Zealand*, volume 205 of *Proceedings of Machine Learning Research*, pages 1893–1903. PMLR, 2022. URL https://proceedings.mlr.press/v205/feng23a.html.

[58] J. Schulman, F. Wolski, P. Dhariwal, A. Radford, and O. Klimov. Proximal policy optimization algorithms. *arXiv preprint arXiv:1707.06347*, 2017.

[59] T. Miki, J. Lee, J. Hwangbo, L. Wellhausen, V. Koltun, and M. Hutter. Learning robust perceptive locomotion for quadrupedal robots in the wild. *Science Robotics*, 7(62):eabk2822, 2022.

[60] G. B. Margolis and P. Agrawal. Walk these ways: Tuning robot control for generalization with multiplicity of behavior. In *Conference on Robot Learning*, pages 22–31. PMLR, 2023.

[61] S. Choi, G. Ji, J. Park, H. Kim, J. Mun, J. H. Lee, and J. Hwangbo. Learning quadrupedal locomotion on deformable terrain. *Science Robotics*, 8(74):eade2256, 2023.

[62] K. Caluwaerts, A. Iscen, J. C. Kew, W. Yu, T. Zhang, D. Freeman, K.-H. Lee, L. Lee, S. Saliceti, V. Zhuang, et al. Barkour: Benchmarking animal-level agility with quadruped robots. *arXiv preprint arXiv:2305.14654*, 2023.

[63] M. Stasica, A. Bick, N. Bohlinger, O. Mohseni, J. Fritzsche, C. Hübler, J. Peters, and A. Seyfarth. Bridge the gap: Enhancing quadruped locomotion with vertical ground perturbations. In *Under review*, 2025. URL https://www.ias.informatik.tu-darmstadt.de/uploads/Team/NicoBohlinger/bridge_the_gap.pdf.

[64] Z. Zhuang, Z. Fu, J. Wang, C. Atkeson, S. Schwertfeger, C. Finn, and H. Zhao. Robot parkour learning. In *Conference on Robot Learning (CoRL)*, 2023.

[65] X. Cheng, K. Shi, A. Agarwal, and D. Pathak. Extreme parkour with legged robots. In *RoboLetics: Workshop on Robot Learning in Athletics@ CoRL 2023*, 2023.

[66] J. Siekmann, K. Green, J. Warila, A. Fern, and J. Hurst. Blind bipedal stair traversal via sim-to-real reinforcement learning. In *Robotics: Science and Systems*, 2021.

[67] A. Kumar, Z. Li, J. Zeng, D. Pathak, K. Sreenath, and J. Malik. Adapting rapid motor adaptation for bipedal robots. In *2022 IEEE/RSJ International Conference on Intelligent Robots and Systems (IROS)*, pages 1161–1168. IEEE, 2022.

[68] I. Radosavovic, T. Xiao, B. Zhang, T. Darrell, J. Malik, and K. Sreenath. Real-world humanoid locomotion with reinforcement learning. *arXiv:2303.03381*, 2023.

[69] Q. Liao, B. Zhang, X. Huang, X. Huang, Z. Li, and K. Sreenath. Berkeley humanoid: A research platform for learning-based control. *arXiv preprint arXiv:2407.21781*, 2024.

[70] Z. Zhuang, S. Yao, and H. Zhao. Humanoid parkour learning. *arXiv preprint arXiv:2406.10759*, 2024.

[71] E. Chane-Sane, J. Amigo, T. Flayols, L. Righetti, and N. Mansard. Soloparkour: Constrained reinforcement learning for visual locomotion from privileged experience. In *8th Annual Conference on Robot Learning*, 2024.

[72] E. Kaufmann, L. Bauersfeld, A. Loquercio, M. Müller, V. Koltun, and D. Scaramuzza. Champion-level drone racing using deep reinforcement learning. *Nature*, 620(7976):982–987, 2023.

[73] A. Kumar, Z. Fu, D. Pathak, and J. Malik. Rma: Rapid motor adaptation for legged robots. *Robotics: Science and Systems XVII*, 2021.

[74] N. Rudin, D. Hoeller, P. Reist, and M. Hutter. Learning to walk in minutes using massively parallel deep reinforcement learning. In *Conference on Robot Learning*, pages 91–100. PMLR, 2022.

[75] G. Margolis, G. Yang, K. Paigwar, T. Chen, and P. Agrawal. Rapid locomotion via reinforcement learning. In *Robotics: Science and Systems*, 2022.

[76] X. B. Peng, M. Andrychowicz, W. Zaremba, and P. Abbeel. Sim-to-real transfer of robotic control with dynamics randomization. In *2018 IEEE international conference on robotics and automation (ICRA)*, pages 3803–3810. IEEE, 2018.

[77] L. Campanaro, S. Gangapurwala, W. Merkt, and I. Havoutis. Learning and deploying robust locomotion policies with minimal dynamics randomization. *arXiv preprint arXiv:2209.12878*, 2022.

[78] L. Smith, I. Kostrikov, and S. Levine. A walk in the park: Learning to walk in 20 minutes with model-free reinforcement learning. *arXiv preprint arXiv:2208.07860*, 2022.

[79] L. Smith, Y. Cao, and S. Levine. Grow your limits: Continuous improvement with real-world rl for robotic locomotion. *arXiv preprint arXiv:2310.17634*, 2023.

[80] J. Levy, T. Westenbroek, and D. Fridovich-Keil. Learning to walk from three minutes of real-world data with semi-structured dynamics models. In *8th Annual Conference on Robot Learning*, 2024.

[81] N. Bohlinger, J. Kinzel, D. Palenicek, L. Antczak, and J. Peters. Gait in eight: Efficient on-robot learning for omnidirectional quadruped locomotion. *arXiv preprint arXiv:2503.08375*, 2025.

[82] F. Jenelten, J. He, F. Farshidian, and M. Hutter. Dtc: Deep tracking control–a unifying approach to model-based planning and reinforcement-learning for versatile and robust locomotion. *arXiv preprint arXiv:2309.15462*, 2023.

[83] M. Kasaei, M. Abreu, N. Lau, A. Pereira, and L. P. Reis. A cpg-based agile and versatile locomotion framework using proximal symmetry loss. *arXiv preprint arXiv:2103.00928*, 2021.

[84] A. Zhao, J. Xu, M. Konaković-Luković, J. Hughes, A. Spielberg, D. Rus, and W. Matusik. Robogrammar: graph grammar for terrain-optimized robot design. *ACM Transactions on Graphics (TOG)*, 39(6):1–16, 2020.

[85] T. Azakami, H. Kera, and K. Kawamoto. Adversarial body shape search for legged robots. In *2022 IEEE International Conference on Systems, Man, and Cybernetics (SMC)*, pages 682–687. IEEE, 2022.

[86] C. Rajani, K. Arndt, D. Blanco-Mulero, K. S. Luck, and V. Kyrki. Co-imitation: learning design and behaviour by imitation. In *Proceedings of the AAAI Conference on Artificial Intelligence*, volume 37, pages 6200–6208, 2023.

[87] C. Hazard, N. Pollard, and S. Coros. Automated design of robotic hands for in-hand manipulation tasks. *International Journal of Humanoid Robotics*, 17(01):1950029, 2020.

[88] A. Gupta, L. Fan, S. Ganguli, and L. Fei-Fei. Metamorph: Learning universal controllers with transformers. *arXiv preprint arXiv:2203.11931*, 2022.

[89] A. Patel and S. Song. Get-zero: Graph embodiment transformer for zero-shot embodiment generalization. *arXiv preprint arXiv:2407.15002*, 2024.

[90] X. Cheng, Y. Ji, J. Chen, R. Yang, G. Yang, and X. Wang. Expressive whole-body control for humanoid robots. In D. Kulic, G. Venture, K. E. Bekris, and E. Coronado, editors, *Robotics: Science and Systems XX, Delft, The Netherlands, July 15-19, 2024*, 2024. doi:10.15607/RSS.2024.XX.107. URL https://doi.org/10.15607/RSS.2024.XX.107.

[91] J. Bjorck, F. Castañeda, N. Cherniadev, X. Da, R. Ding, Linxi, Y. Fang, D. Fox, F. Hu, S. Huang, J. Jang, Z. Jiang, J. Kautz, K. Kundalia, L. Lao, Z. Li, Z. Lin, K. Lin, G. Liu, E. LLontop, L. Magne, A. Mandlekar, A. Narayan, S. Nasiriany, S. Reed, Y. L. Tan, G. Wang, Z. Wang, J. Wang, Q. Wang, J. Xiang, Y. Xie, Y. Xu, Z. Xu, S. Ye, Z. Yu, A. Zhang, H. Zhang, Y. Zhao, R. Zheng, and Y. Zhu. GR00T N1: an open foundation model for generalist humanoid robots. *CoRR*, abs/2503.14734, 2025. doi:10.48550/ARXIV.2503.14734. URL https://doi.org/10.48550/arXiv.2503.14734.

[92] M. Ji, X. Peng, F. Liu, J. Li, G. Yang, X. Cheng, and X. Wang. Exbody2: Advanced expressive humanoid whole-body control. *CoRR*, abs/2412.13196, 2024. doi:10.48550/ARXIV.2412.13196. URL https://doi.org/10.48550/arXiv.2412.13196.

[93] C. Sferrazza, D. Huang, X. Lin, Y. Lee, and P. Abbeel. Humanoidbench: Simulated humanoid benchmark for whole-body locomotion and manipulation. In D. Kulic, G. Venture, K. E. Bekris, and E. Coronado, editors, *Robotics: Science and Systems XX, Delft, The Netherlands, July 15-19, 2024*, 2024. doi:10.15607/RSS.2024.XX.061. URL https://doi.org/10.15607/RSS.2024.XX.061.

[94] H. Shi, W. Wang, S. Song, and C. K. Liu. Toddlerbot: Open-source ml-compatible humanoid platform for loco-manipulation, 2025. URL https://arxiv.org/abs/2502.00893.

[95] M. Liu, Z. Chen, X. Cheng, Y. Ji, R. Qiu, R. Yang, and X. Wang. Visual whole-body control for legged loco-manipulation. In P. Agrawal, O. Kroemer, and W. Burgard, editors, *Conference on Robot Learning, 6-9 November 2024, Munich, Germany*, volume 270 of *Proceedings of Machine Learning Research*, pages 234–257. PMLR, 2024. URL https://proceedings.mlr.press/v270/liu25b.html.

[96] R. Yang, M. Zhang, N. Hansen, H. Xu, and X. Wang. Learning vision-guided quadrupedal locomotion end-to-end with cross-modal transformers. In *The Tenth International Conference on Learning Representations, ICLR 2022, Virtual Event, April 25-29, 2022*. OpenReview.net, 2022. URL https://openreview.net/forum?id=nhnJ3oo6AB.

[97] T. He, C. Zhang, W. Xiao, G. He, C. Liu, and G. Shi. Agile but safe: Learning collision-free high-speed legged locomotion. In D. Kulic, G. Venture, K. E. Bekris, and E. Coronado, editors, *Robotics: Science and Systems XX, Delft, The Netherlands, July 15-19, 2024*, 2024. doi:10.15607/RSS.2024.XX.059. URL https://doi.org/10.15607/RSS.2024.XX.059.

[98] G. B. Margolis, G. Yang, K. Paigwar, T. Chen, and P. Agrawal. Rapid locomotion via reinforcement learning. *Int. J. Robotics Res.*, 43(4):572–587, 2024. doi:10.1177/02783649231224053. URL https://doi.org/10.1177/02783649231224053.

[99] J. Tan, T. Zhang, E. Coumans, A. Iscen, Y. Bai, D. Hafner, S. Bohez, and V. Vanhoucke. Sim-to-real: Learning agile locomotion for quadruped robots. In H. Kress-Gazit, S. S. Srinivasa, T. Howard, and N. Atanasov, editors, *Robotics: Science and Systems XIV, Carnegie Mellon University, Pittsburgh, Pennsylvania, USA, June 26-30, 2018*, 2018. doi:10.15607/RSS.2018.XIV.010. URL http://www.roboticsproceedings.org/rss14/p10.html.

[100] H. Zhang, Y. Liu, J. Zhao, J. Chen, and J. Yan. Development of a Bionic Hexapod Robot for Walking on Unstructured Terrain. *Journal of Bionic Engineering*, 11(2):176–187, June 2014. ISSN 2543-2141. doi:10.1016/S1672-6529(14)60041-X. URL https://doi.org/10.1016/S1672-6529(14)60041-X.

[101] Z. Zang, M. Kawawa-Beaudan, W. Yu, T. Zhang, and A. Zakhor. Perceptive Hexapod Legged Locomotion for Climbing Joist Environments. In *2023 IEEE/RSJ International Conference on Intelligent Robots and Systems (IROS)*, pages 2738–2745, Detroit, MI, USA, Oct. 2023. IEEE. ISBN 978-1-66549-190-7. doi:10.1109/IROS55552.2023.10341957. URL https://ieeexplore.ieee.org/document/10341957/.

[102] T. Qu, D. Li, A. Zakhor, W. Yu, and T. Zhang. Versatile locomotion skills for hexapod robots. In *2024 IEEE/RSJ International Conference on Intelligent Robots and Systems (IROS)*, pages 6885–6892, 2024. doi:10.1109/IROS58592.2024.10801714.

[103] W. Ouyang, H. Chi, J. Pang, W. Liang, and Q. Ren. Adaptive locomotion control of a hexapod robot via bio-inspired learning. *Frontiers Neurorobotics*, 15:627157, 2021. doi:10.3389/FNBOT.2021.627157. URL https://doi.org/10.3389/fnbot.2021.627157.

[104] T. Azayev and K. Zimmerman. Blind Hexapod Locomotion in Complex Terrain with Gait Adaptation Using Deep Reinforcement Learning and Classification. *J Intell Robot Syst*, 2020.

[105] J.-R. Chiu, Y.-C. Huang, H.-C. Chen, K.-Y. Tseng, and P.-C. Lin. Development of a Running Hexapod Robot with Differentiated Front and Hind Leg Morphology and Functionality. In *2020 IEEE/RSJ International Conference on Intelligent Robots and Systems (IROS)*, pages 3710–3717, Las Vegas, NV, USA, Oct. 2020. IEEE. doi:10.1109/iros45743.2020.9340811. URL https://ieeexplore.ieee.org/document/9340811/.

[106] Haitao Yu, Wei Guo, Jing Deng, Mantian Li, and Hegao Cai. A CPG-based locomotion control architecture for hexapod robot. In *2013 IEEE/RSJ International Conference on Intelligent Robots and Systems*, pages 5615–5621, Tokyo, Nov. 2013. IEEE. doi:10.1109/iros.2013.6697170. URL http://ieeexplore.ieee.org/document/6697170/.

[107] A. Vaswani, N. Shazeer, N. Parmar, J. Uszkoreit, L. Jones, A. N. Gomez, L. Kaiser, and I. Polosukhin. Attention is all you need. In *Proceedings of the 31st International Conference on Neural Information Processing Systems*, NIPS'17, page 6000–6010, Red Hook, NY, USA, 2017. Curran Associates Inc. ISBN 9781510860964.

[108] M. Mittal, C. Yu, Q. Yu, J. Liu, N. Rudin, D. Hoeller, J. L. Yuan, R. Singh, Y. Guo, H. Mazhar, A. Mandlekar, B. Babich, G. State, M. Hutter, and A. Garg. Orbit: A unified simulation framework for interactive robot learning environments. *IEEE Robotics and Automation Letters*, 8(6):3740–3747, 2023. doi:10.1109/LRA.2023.3270034.

[109] L. van der Maaten and G. Hinton. Visualizing data using t-sne. *Journal of Machine Learning Research*, 9(86):2579–2605, 2008. URL http://jmlr.org/papers/v9/vandermaaten08a.html.

[110] I. Jolliffe. *Principal component analysis*. Springer Verlag, New York, 2002.

[111] L. McInnes and J. Healy. UMAP: uniform manifold approximation and projection for dimension reduction. *CoRR*, abs/1802.03426, 2018. URL http://arxiv.org/abs/1802.03426.

[112] I. Loshchilov and F. Hutter. Decoupled weight decay regularization. In *7th International Conference on Learning Representations, ICLR 2019, New Orleans, LA, USA, May 6-9, 2019*. OpenReview.net, 2019. URL https://openreview.net/forum?id=Bkg6RiCqY7.

[113] I. Loshchilov and F. Hutter. SGDR: stochastic gradient descent with warm restarts. In *5th International Conference on Learning Representations, ICLR 2017, Toulon, France, April 24-26, 2017, Conference Track Proceedings*. OpenReview.net, 2017. URL https://openreview.net/forum?id=Skq89Scxx.

Appendix

A Expert Training

A.1 Observation and Action Space

The observation space of the expert policies includes the joint angles, joint velocities, previous actions, trunk angular velocities, gravity vector and the command velocities. The observation space of the critics includes the same observations as for the policies, but also includes privileged information: the trunk linear velocity, trunk height over the ground, feet contact states and feet air times.

The policies control the robots at 50 Hz with a PD controller, where the target joint angles are generated by scaling the action of the policy and adding it to the nominal joint configuration of the robot: $q_{\text{target}} = q_{\text{nominal}} + \sigma \cdot a$. We define the nominal joint configuration as a standing pose of a robot and use the same configuration for all robots of the same morphology class (see Appendix B.3). For the action scaling factor σ, we use 0.3 for quadrupeds and hexapods, and 0.75 for humanoids. For the PD controller, we use $K_p = 20$ and $K_d = 0.5$ for quadrupeds, $K_p = 25$ and $K_d = 0.5$ for hexapods, and $K_p = 60$ and $K_d = 2.0$ for humanoids.

A.2 Domain Randomization

To enable sim-to-real transfer of the trained policies, we add strong domain randomization during training. We use a performance-based curriculum learning approach, where the domain randomization ranges are increased from 0 (or their mean if not zero-centered) to the final values in Table 1 over the course of training. This curriculum approach allows the policy to learn basic locomotion first in the simplest possible environment before adapting to wider variations. We define a curriculum coefficient from 0 to 1, which is multiplied with the domain randomization ranges (and the reward penalty coefficients). The coefficient of an environment is increased by 0.01 if the policy completed the episode without falling, and the average tracking error of the target x,y velocity is below 0.4 m/s, and the coefficient is reduced by 0.01 otherwise.

Every embodiment in GENBOT-1K uses the same domain randomization ranges. The "starting" values (naming scheme in Table 1) are sampled uniformly at the start of every episode to randomize the starting state of the robot. The "noise" values are sampled uniformly for every simulation step to add noise to the observations. The values of every other parameter are sampled uniformly every simulation step with a probability of 0.002 (on average every 500 steps / every 10 seconds). Pushes are applied as linear velocities to the trunk of the robot.

Table 1: **Domain randomization configuration.** Domain randomization values and ranges for every randomized parameter during the expert RL training. The values in the table are the maximum values and ranges in the curriculum when reaching the final curriculum coefficient of 1.

Parameter	Value
Max action delay	1
Chance for action delay	0.05
Min & max motor strength	(0.5, 1.5)
Min & max P gain factor	(0.5, 1.5)
Min & max D gain factor	(0.5, 1.5)
Min & max joint position offset	(-0.05, 0.05)
Min & max starting orientation factor	(-0.0625, 0.0625)
Min & max starting joint position factor	(-0.5, 0.5)
Min & max starting joint velocity factor	(-0.5, 0.5)
Min & max starting linear velocity	(-0.5, 0.5)
Min & max starting angular velocity	(-0.5, 0.5)
Joint position noise	0.01
Joint velocity noise	1.5
Angular velocity noise	0.2
Gravity velocity noise	0.05
Joint observation dropout chance	0.05
Min & max static friction	(0.05, 2.0)
Min & max dynamic friction	(0.05, 1.5)
Min & max restitution	(0.0, 1.0)
Min & max added mass	(-2.0, 2.0)
Min & max gravity	(-8.81, 10.81)
Min & max joint friction	(0.0, 0.01)
Min & max joint armature	(0.0, 0.01)
Min & max pushes in x	(-1.0, 1.0)
Min & max pushes in y	(-1.0, 1.0)
Min & max pushes in z	(-1.0, 1.0)

A.3 Reward Function

Table 2 contains all reward terms and coefficients of the reward function for the expert training of all robots in the GENBOT-1K dataset. Joint-based (T6-T12) and feet-based (T14-T17) reward terms are calculated as the mean over every joint and foot, respectively, to account for the varying amounts of joints and feet of the generated embodiments. The coefficients of all penalties are attached to the curriculum coefficient (see Appendix A.2) and thus linearly increase from 0 to the final values in Table 2 over the course of training. This makes the training process less sensitive to the precise values of the coefficients.

Table 2: **Reward terms for the RL training of embodiment-specific experts.** All reward terms and the corresponding coefficients that compose the reward function for the expert training. While all the coefficients work for all embodiments, for the final experiments, we tweaked four coefficients for the humanoid embodiments to improve the style of the gait: [*1] 3.0, [*2] 1.5, [*3] 43.2, [*4] 6e-3.

	Term	Equation	Coefficient
T1	Xy velocity tracking	$\exp(-\lvert v_{xy} - c_{xy}\rvert^2/0.25)$	2.0 [*1]
T2	Yaw velocity tracking	$\exp(-\lvert \omega_{\text{yaw}} - c_{\text{yaw}}\rvert^2/0.25)$	1.0 [*2]
T3	Z velocity penalty	$-\lvert v_z\rvert^2$	2.0
T4	Pitch-roll velocity penalty	$-\lvert \omega_{\text{pitch, roll}}\rvert^2$	0.05
T5	Pitch-roll position penalty	$-\lvert \theta_{\text{pitch, roll}}\rvert^2$	5.0
T6	Joint nominal differences penalty	$-\lvert q - q^{\text{nominal}}\rvert^2$	14.4 [*3]
T7	Joint position limits penalty	$-\bar{\mathbb{1}}(0.9q_{\text{min}} < q < 0.9q_{\text{max}})$	120.0
T8	Joint velocity limits penalty	$-\bar{\mathbb{1}}(0.9\dot{q}_{\text{min}} < \dot{q} < 0.9\dot{q}_{\text{max}})$	10.0
T9	Joint accelerations penalty	$-\lvert \ddot{q}\rvert^2$	5e-6
T10	Joint torques penalty	$-\lvert \tau\rvert^2$	2.4e-4
T11	Action rate penalty	$-\lvert a_t - a_{t-1}\rvert^2$	0.12
T12	Action smoothness penalty	$-\lvert a_t - 2a_{t-1} + a_{t-2}\rvert^2$	0.12
T13	Walking height penalty	$-\lvert h - h_{\text{nominal}}\rvert^2$	30.0
T14	Air time penalty	$-\sum_f \mathbb{1}(p_f)(p_f^T - 0.5)$	0.1
T15	Symmetry penalty	$-\sum_f \bar{\mathbb{1}}(p_f^{\text{left}})\bar{\mathbb{1}}(p_f^{\text{right}})$	0.5
T16	Feet y distance penalty	$-\lvert f^{\text{actual}}_{\text{y distance}} - f^{\text{target}}_{\text{y distance}}\rvert^2$	2.0
T17	Feet force penalty	$-\lvert f_{\text{force}}\rvert^2$	8e-3 [*4]
T18	Self-collision penalty	$-\mathbb{1}_{\text{self-collision}}$	1.0

A.4 PPO Hyperparameters

We use the same PPO hyperparameters for the training of all expert policies, detailed in Table 3. Searching for better hyperparameters for every embodiment might lead to increased performance but is impractical when considering training $\sim$1000 embodiments. The chosen hyperparameters are based on common practices in legged locomotion research [41, 74] and preliminary tuning on a small subset of embodiments.

Table 3: **PPO hyperparameters for expert policy training.**

Hyperparameter	Value
Batch size	98304
Mini-batch size	24576
# epochs	5
Initial learning rate	0.001
Learning rate schedule	Adaptive with target KL 0.01
Entropy coefficient	0.002
Discount factor	0.99
GAE λ	0.95
Clip range	0.2
Max gradient norm	1.0
Initial action standard deviation	1.0
Clip range action mean	-10.0, 10.0
Policy and critic hidden layers	[512, 256, 128]
Activation function	ELU
# training iterations	17500 (quadruped, hexapod), 42500 (humanoid)

B Embodiment Generation

B.1 Basic Units for Quadruped, Humanoid and Hexapod

Tables 4 and 5 provide the base values for geometry-related and kinematics-related parameters, respectively, for representative links across quadruped, humanoid, and hexapod morphologies. For the humanoid class, we report parameters for the trunk and the left-side lower-body links. For quadruped and hexapod classes, we include the front-left leg. The remaining components are either symmetric or peripheral to locomotion (e.g., arms or head for humanoids) and therefore omitted.

The base parameter values are partially inspired by the Unitree Go2 and H1 platforms, offering a degree of realism without exact replication. This design choice is consistent with prior work such as GenLoco [57], which abstracts physical characteristics from real robots to define a diverse yet grounded design space. Robots instantiated with these values correspond to a $1.0\times$ variation setting (i.e., no geometric, kinematic, or topological scaling applied), and serve as the reference point for applying the variation factors listed in Tables 4 and 5.

To support meaningful evaluation of generalization, these reference robots are excluded from the training set. Every robot in the training set differs from Go2 and H1 by at least one geometric, topological, or kinematic variation, along with additional discrepancies due to loose alignment in parameter values (e.g., each joint in the humanoid closest to H1 differs by a few centimeters, and the overall height differs by approximately 10 cm). This diversity encourages the learned policy to capture broadly transferable motion patterns. As discussed in Section 4, empirical results suggest that the policy has acquired sufficiently generalizable behaviors to support both cross-embodiment and sim-to-real transfer, which is generally considered highly challenging.

B.2 Generation Algorithm

We construct each robot embodiment in a tree-like structure by iteratively connecting links using joints, following the URDF specification and the basic units described in Section B.1. The construction procedure varies slightly across morphologies:

- **Humanoids**: The root node is the pelvis. We first append the torso and hip links, then attach the shoulder and arm links for the upper body, followed by the thigh, calf, and foot links for the lower body.
- **Quadrupeds and hexapods**: The root node is the trunk. We sequentially append the hip links to the trunk, then connect the leg and foot links to form the complete body.

To ensure diversity in the generated embodiments, we introduce variations in geometry, topology, and kinematics during the construction process, as detailed in Section 3. Table 6 summarizes the variation parameters and their corresponding candidate values. While most parameters are self-explanatory, we clarify a few specific cases:

- **Number of knee joints**: If a leg is configured with zero knee joints, the calf link is omitted, and the thigh link is directly connected to the foot.
- **Foot link size**: For humanoids, foot links are modeled as boxes and scaled by length; for quadrupeds and hexapods, foot links are modeled as spheres and scaled by radius.
- **Joint limit variation**: Joint limits are varied by uniformly scaling the nominal joint ranges about the nominal joint position, which serves as a fixed point.

B.3 Nominal Joint Configurations

Nominal joint configurations are used to initialize robot poses during training, contribute to reward terms that discourage deviations too far from these default joint angles, and function as offsets to the actions of the expert and distillation policies. As such, they serve as useful regularizers for learning realistic and efficient gaits. To support scalability across diverse morphologies, we generate nominal

configurations by reusing unit values across the generated embodiments. The nominal joint angles used are summarized in Table 7.

Table 4: **Base geometry and mass parameters for representative link types in the embodiment generation pipeline used in GENBOT-1K.** Geometry dimensions are specified according to shape type: Sphere (radius), Cylinder (length, radius), and Box (length, width, height).

Class	Link Name	Geometry Type	Geometry Dimension (m)	Mass (kg)
Humanoid	Pelvis	Sphere	(0.05,)	5.390
	Torso	Box	(0.08, 0.26, 0.18)	17.789
	Hip yaw link	Cylinder	(0.02, 0.01)	2.244
	Hip roll link	Cylinder	(0.01, 0.02)	2.232
	Thigh	Cylinder	(0.2, 0.05)	4.152
	Calf	Cylinder	(0.2, 0.05)	1.721
	Foot	Box	(0.28, 0.03, 0.024)	0.474
Quadruped	Trunk	Box	(0.38, 0.09, 0.11)	6.921
	Hip	Cylinder	(0.04, 0.046)	1.152
	Thigh	Box	(0.21, 0.025, 0.034)	1.152
	Calf	Cylinder	(0.12, 0.013)	0.154
g	Foot	Sphere	(0.022,)	0.040
Hexapod	Trunk	Box	(0.8, 0.5, 0.1)	6.921
	Hip	Sphere	(0.05,)	0.678
	Thigh	Cylinder	(0.22, 0.03)	1.152
	Calf	Cylinder	(0.22, 0.025)	0.154
	Foot	Sphere	(0.03,)	0.040

Table 5: **Motor and joint properties of the generated embodiments in GENBOT-1K.**

Class	Joint Name	Joint Limits (rad)	Max. Torque (N·m)	Max. Velocity (rad/s)
Humanoid	Torso joint	(-2.35, 2.35)	200	23
	Shoulder pitch joint	(-2.87, 2.87)	40	9
	Shoulder roll joint	(-0.34, 3.11)	40	9
	Shoulder yaw joint	(-1.30, 4.45)	18	20
	Elbow joint	(-1.25, 2.61)	18	20
	Hip yaw/roll joint	(-0.43, 0.43)	200	23
	Hip pitch	(-3.10, 2.50)	200	23
	Knee joint	(-0.26, 2.00)	300	14
	Ankle joint	(-0.87, 0.52)	40	9
Quadruped	Hip pitch joint	(-1.05, 1.05)	23.7	30.1
	Front thigh joint	(-1.57, 3.49)	23.7	30.1
	Rear thigh joint	(-0.52, 4.53)	23.7	30.1
	Knee joint	(-2.72, -0.84)	45.43	15.7
Hexapod	Hip joint	(-1.57, 1.57)	100	30
	Thigh joint	(-1.57, 1.57)	100	30
	Knee joint	(-1.57, 1.57)	100	30

Table 6: **Variation parameters across geometry, topology, and kinematics in the embodiment generation algorithm.** The torso link randomization only applicable to the humanoid class.

Variation Type	Parameter Name	Candidate Values
Topology	Number of knee joints	{0, 1, 2, 3}
Geometry	Scaling factor for all link size	{0.8, 1.0, 1.2}
	Scaling factor for thigh link length	{0.4, 0.8, 1.0, 1.2, 1.6}
	Scaling factor for calf link length	{0.4, 0.8, 1.0, 1.2, 1.6}
	Scaling factor for foot link size	{1.0, 2.0}
	Scaling factor for torso link size	{0.4, 0.8, 1.0, 1.2, 1.6}
Kinematics	Scaling factor for knee joint limits	{0.2, 0.6, 1.0}

Table 7: **Nominal joint configurations for generated embodiments in GENBOT-1K.** These joint angles are used to initialize robot poses, define regularization rewards, and function as offsets to the policy actions. The values are consistent across symmetric limbs.

Class	Joint Name	Joint Angle (rad)
Humanoid	Torso	0.0
	Shoulder (Left/Right, pitch/roll/yaw)	0.0
	Elbow (Left/Right)	0.0
	Hip pitch (Left/Right)	-0.4
	Hip roll/yaw (Left/Right)	0.0
	Knee (Left/Right)	0.8
	Ankle (Left/Right)	-0.4
Quadruped	Hip (Front/Rear, Left/Right)	± 0.1
	Thigh (Front, Left/Right)	0.8
	Thigh (Rear, Left/Right)	1.0
	Knee (Front/Rear, Left/Right)	-1.5
	Additional knee joints (if any)	0.0
Hexapod	Hip (Front/Middle/Rear, Left/Right)	0.0
	Thigh (Front/Middle/Rear, Left/Right)	0.79
	Knee (Front/Middle/Rear, Left/Right)	0.79
	Additional knee joints (if any)	0.0

C Cross-Embodiment Distillation

C.1 Expert Data Collection

For every embodiment, we run the expert RL policy for 600 simulation steps using 4096 parallel environments. This results in a total of 1,985,740,800 data samples across all training embodiments. Note that the episode length during the expert training is 1000 simulation steps (equivalent to 20 physical seconds), thus, the collected data only covers the first half of the episode. Using the full length may provide more time-correlated data, which we did not analyze due to time constraints. The final dataset needs around 5 TB of storage using the `h5py` format without additional compression.

C.2 URMA Architecture Details

The observation space of the URMA policy is split into two parts: joint-specific observations o_j and general observations o_g. The joint-specific observations o_j include the joint angle, joint velocity, previous action of the joint (shape: $(j(e), 3)$). The general observations o_g include the trunk linear velocity, gravity vector, command velocities, PD gains, action scaling factor, total mass of the robot, robot dimensions, number of joints and feet size (shape: (20,)).

The description vectors d_j of the joints include the relative carthesian position of the joint in the nominal configuration, joint rotation axis, joint nominal angle, maximum joint torque, maximum joint velocity, joint position limits, p-gain, d-gain and action scaling factor, robot mass and dimensions (shape: $(j(e), 18)$).

We build on the original URMA neural network architecture, as shown in Figure 7, from Bohlinger et al. [41] with the following modifications:

- We use multi-headed attention for the encoding of the joint observations and descriptions to increase the expressiveness of the policy. All our experiments use 3 attention heads.
- We remove the feet-specific attention encoder as not all robots in the real world have foot-specific sensors, like pressure sensors.
- We directly use the output from the action decoder μ_ν as the action of the policy, instead of using an additional head to produce a standard deviation and sampling from a Gaussian distribution, as we train the policy with imitation learning instead of RL.
- We add another encoding layer to the general observations o_g to project them into a higher dimensional latent space before concatenating them with all the joint latent vectors from the attention heads.
- We use wider feedforward layers ($2\times$ the hidden dimensions) throughout the network.

The resulting model has 2.1 million parameters. Overall, it is a compact network with strong inductive biases that leverage the compositional structure of robots.

When applying the actions of the policy to the robots, we use the same PD controllers with the same nominal joint configurations and action scaling factors as in the expert training (see Appendix A.1).

C.3 Train-Test Set Splits

We split GENBOT-1K into a training set (80%) and a test set (20%) using a deterministic pseudo-random sampler with a fixed seed, ensuring full reproducibility. The same sampling procedure is applied independently to each morphology class, except for quadrupeds and hexapods, which share identical splits due to matched dataset sizes. Detailed test indices are listed in Table 8, and summary statistics for each category are shown in Table 9.

Table 8: **Train-test splits of GENBOT-1K.** Each index refers to one unique embodiment in each embodiment class. The training set is simply the complement of the test set and thus omitted.

Class	Test Set
Humanoid	[0, 7, 12, 20, 31, 32, 37, 41, 46, 47, 48, 50, 51, 55, 63, 71, 72, 75, 97, 104, 111, 113, 122, 124, 128, 132, 133, 144, 149, 154, 155, 158, 161, 163, 166, 169, 170, 181, 183, 197, 204, 207, 215, 222, 226, 229, 241, 244, 248, 250, 252, 258, 260, 261, 266, 272, 276, 278, 280, 282, 286, 290, 298, 308, 312, 313, 316, 320, 327, 342]
Quadruped	[0, 7, 8, 20, 31, 32, 37, 41, 46, 47, 48, 50, 51, 55, 71, 72, 75, 97, 104, 111, 113, 122, 124, 128, 132, 133, 144, 149, 154, 155, 158, 161, 163, 166, 169, 170, 181, 183, 197, 204, 207, 215, 222, 226, 229, 241, 244, 248, 250, 252, 258, 260, 261, 266, 272, 278, 280, 282, 286, 290, 298, 308, 312, 313, 316, 320, 327]
Hexapod	[0, 7, 8, 20, 31, 32, 37, 41, 46, 47, 48, 50, 51, 55, 71, 72, 75, 97, 104, 111, 113, 122, 124, 128, 132, 133, 144, 149, 154, 155, 158, 161, 163, 166, 169, 170, 181, 183, 197, 204, 207, 215, 222, 226, 229, 241, 244, 248, 250, 252, 258, 260, 261, 266, 272, 278, 280, 282, 286, 290, 298, 308, 312, 313, 316, 320, 327]

Table 9: **Statistics of train-test splits of GENBOT-1K.** The splits have an approximately balanced distribution over different categories.

Class	Total Number	Train Set (80%)	Test Set (20%)
Humanoid	348	278	70
Quadruped	332	265	67
Hexapod	332	265	67
Total	1012	808	204

C.4 Training Details

We designed an efficient training pipeline that balances disk I/O, CPU preprocessing, GPU utilization, and RAM usage. Instead of loading every minibatch directly from disk, we first load a fixed number of data slices, each containing a small subset of steps from multiple robot embodiments, into an in-memory buffer. Each slice consists of 100 trajectories with 128 steps per trajectory. Once the buffer is filled, minibatches are sampled uniformly at random, without replacement, until every sample has been seen a fixed number of times. This strategy reduces disk access overhead, improves memory locality, and maintains sample diversity throughout training, though it may introduce local overfitting and biased gradient estimates.

Because data from different robots have varied observation and action spaces, we load them separately and use gradient accumulation to reduce bias in the gradient estimation. Specifically, gradients are accumulated across multiple minibatches before each optimizer step, helping to balance contributions across robot embodiments. While effective, this approach still suffers from local gradient bias. A more principled solution would involve zero-padding to form large, uniform batches across robots, but implementing this would require architectural and pipeline-level changes, which we did not pursue due to time constraints. In theory, this could lead to smoother optimization and potentially better final performance.

To ensure numerical stability, we apply gradient clipping with a maximum norm of 5. We use the AdamW optimizer [112] with β_1=0.9, β_2=0.999, and a cosine-annealed weight decay schedule that decays from 3×10^{-4} to 0 over the course of training [113]. The key hyperparameters for distillation are summarized in Table 10.

Our pipeline requires 128 GB of RAM to maintain the in-memory buffer. Due to the small size of the URMA policy, training can be efficiently performed on a single GPU (e.g., NVIDIA RTX 4090 or H100). We did not observe significant gains in convergence from increasing batch size, possibly

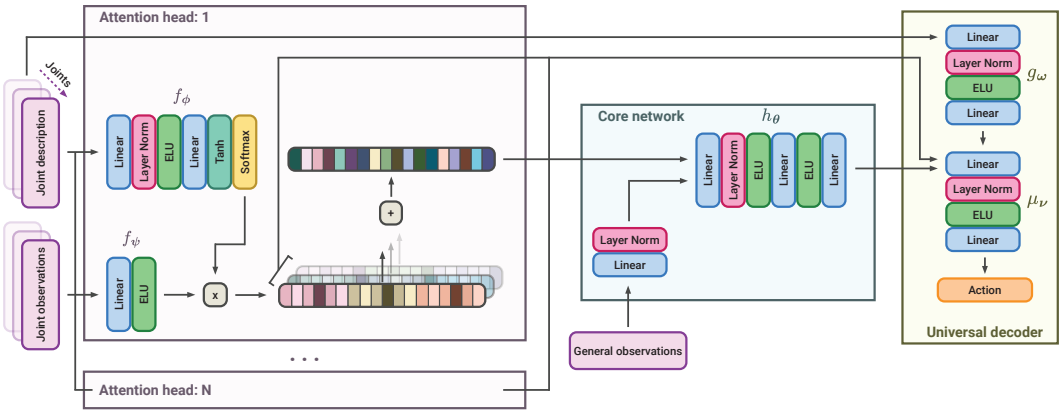

Figure 7: **URMA with multi-head attention.** We extend the original URMA module [41] with multiple attention heads, each aggregating information from joint observations using distinct attention distributions. This design enables the model to capture multi-modal dependencies and improves its capacity to scale across diverse embodiments.

Table 10: **Hyperparameters of the distillation pipeline.**

Hyperparameter	Value
# training samples per embodiment	500×4096
Validation set size	100×4096
Batch size	64
Gradient accumulation steps	8
Gradient clipping threshold	5
Data slice size	100×128
Max slices in buffer	1024
Buffer repeat factor	3
Optimizer	AdamW [112]
AdamW betas	$(0.9,\ 0.999)$
Weight decay schedule	$3 \times 10^{-4} \rightarrow 0$ (cosine)
Learning rate schedule	Cosine annealing [113]
# epochs	80

due to the structured nature and potential bottlenecks in the model architecture. Further investigation into the scaling behavior of the training dynamics is left for future work.

D Additional Results on Out-of-Domain Generalization

Table 11: **Mean reward by knee-range scale.** Values at 0.6 and 0.2 are from GENBOT-1K; values at 0.1 and 0.001 are from the modified version.

Class	0.6	0.2	0.1	0.001
Humanoid	19	14	16	4
Quadruped	49	36	45	26
Hexapod	34	21	28	20

We evaluate out-of-distribution (OOD) generalization by testing the URMA policy trained on GENBOT-1K against a modified test distribution with significantly reduced knee joint limits—{0.1, 0.001}, which lie outside the training range of {0.6, 0.2}. Table 11 reports the mean episode reward across morphology classes at each joint limit scale.

Results show that moderate tightening (0.1) induces only mild performance degradation across all classes. In contrast, extreme tightening (0.001) leads to a sharp drop for the less stable humanoid class, while quadrupeds and hexapods remain more robust. These results highlight the policy's ability to generalize to structurally OOD embodiments, albeit with limitations under severe distributional shift. While expanding the training distribution to cover a broader range of joint configurations could improve robustness, such exploration is beyond the scope of this study.

E Additional Details on Real-World Deployment

E.1 Hardware Setup

We evaluated our distilled URMA policy zero-shot on two real-world platforms: the Unitree Go2 quadruped and the Unitree H1 humanoid. For each robot, we used its URDF to produce the embodiment description vectors d_j. Before deployment, the policy was converted to the ONNX format to load it in JAX and guarantee maximum inference speed. The policy inference ran on a Ubuntu 22.04 laptop (Ryzen 9 CPU), interfaced to the robot over a dedicated Ethernet connection. We ran the control loop at the same 50 Hz and with the same PD gains as in simulation, and sent the target joint angles to the robot's internal controller. We limited the commanded x-y-yaw velocity to 0.8 m/s for the Go2 and 0.5 m/s for the H1, to ensure the robot's stability and safety during the experiments.

E.2 Implementing Joint Limit Variations

To probe robustness under kinematic constraints, we impose an artificial knee-joint range limited to 20, 40 or 60 % of its nominal range. In simulation, one can enforce such limits by directly clamping joint angles within the physics engine; in hardware, however, neither the robot's encoders nor its embedded PD controller can be modified. Consequently, we introduce a software-level joint-limit layer into the control loop in order to restrict the target joint angle for affected knee joints to the new limits. At each control step, the policy's commanded knee angle is constrained to the prescribed ±20, 40 or 60 % bounds. Instead, we implemented a software-based solution that restricts the target joint angle for affected knee joints to the new limits. To counteract any excursions driven by external disturbances, we implement an active rejection mechanism: whenever the measured knee angle violates the software limits, we (1) project the commanded target onto the nearest permissible bound and (2) elevate the proportional and derivative gains to $K_p = 60$ and $K_d = 1$, respectively, until the joint re-enters the safe region. This procedure enforces a soft joint-limit constraint exclusively in software—without altering hardware or contravening physical laws—while delivering high-gain corrective action against environmental perturbations.

F Additional Latent Space Analysis

In addition to the t-SNE analysis, we also apply Principal Component Analysis (PCA) [110] and Uniform Manifold Approximation and Projection (UMAP) [111] on the action latent vectors $\bar{z}_{\text{action}}$ in Figure 8. Both PCA and UMAP projections reveal clear grouping according to the morphology class, with humanoid, quadruped, and hexapod embeddings forming distinct clusters. Compared to the t-SNE analysis, clusters about the topological, geometric, and kinematic variations are less pronounced and appear to be more cramped.

Furthermore, we show in Figure 9 the t-SNE analysis of the learned joint description latent space $f_\phi(d_j)$ for all joints from all embodiments in the GenBot-1K dataset. Although the three morphologies still define the rough structure of this latent space, the learned embeddings for the joint descriptions seem to be much more entangled across the three morphology classes.

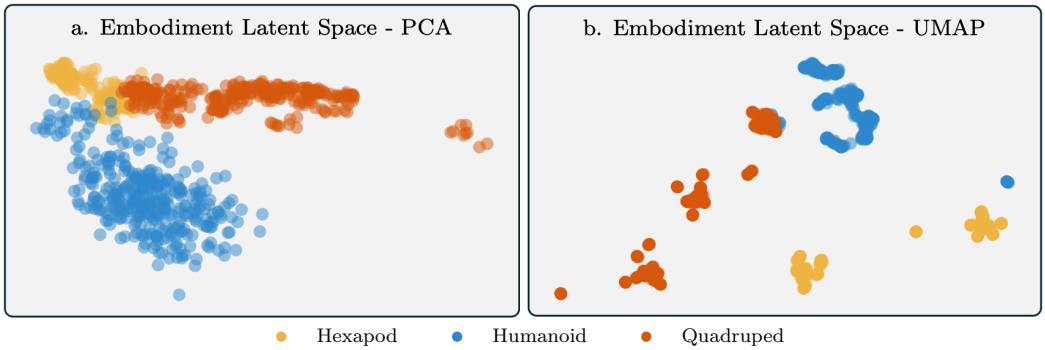

Figure 8: **Additional visualizations of the learned embodiment embeddings.** PCA (a.) and UMAP (b.) of the embodiment latent space (i.e., every point represents one robot, aggregated from all of its joint description vectors).

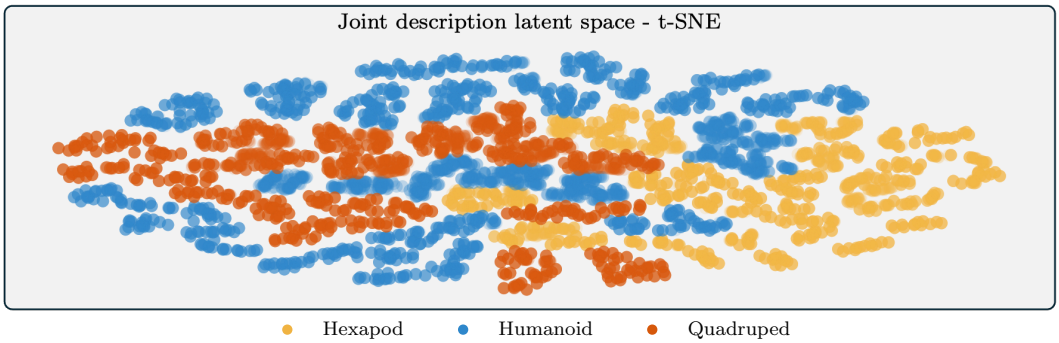

Figure 9: **Additional visualizations of the learned joint description embeddings.** t-SNE visualization of the joint description latent space of all joints from all embodiments in the GENBOT-1K dataset (i.e., every point represents one joint of a robot).